PERIODICO di MINERALOGIA
established in 1930

DIPARTIMENTO
DI SCIENZE DELLA TERRA

SAPIENZA
UNIVERSITÀ DI ROMA

An International Journal of
Mineralogy, Crystallography, Geochemistry,
Ore Deposits, Petrology, Volcanology
and applied topics on Environment, Archaeometry and Cultural Heritage

Titanite-centered ocellar texture:A petrological tool to unravel the mechanism enhancing magma mixing

Bibhuti Gogoi [a], Ashima Saikia [a,*], Mansoor Ahmad [b]

[a] Department of Geology, University of Delhi, New Delhi 110007, India
[b] Rajabazar, Patna 800020, India

ARTICLE INFO

Submitted: April 2017
Accepted: August 2017
Available on line: October 2017

* Corresponding author:
ashima.saikia@gmail.com

DOI: 10.2451/2017PM727

How to cite this article:
Gogoi B. (2017)
Period. Mineral. 86, 247-276

ABSTRACT

The titanite-centered ocellar texture is a rarely observed texture from magma mixing and mingling zones. This work provides a synthesis of petrographical observations and mineral-chemical data to understand the genesis of this texture. The rock with titanite ocelli is from the mafic-felsic interaction zone of the Nimchak Granite Pluton (NGP) of Chotanagpur Granite Gneiss Complex (CGGC) of Eastern India. Interpretations reveal that when mafic (basaltic) magma intrudes in to a crystallizing felsic (granite) magma chamber the early interaction that takes place between the two phases is diffusion of heat from the relatively hotter mafic magma to the colder felsic magma followed by diffusion of elements. When thermal equilibrium is reached between the two magmas their rheological contrasts are drastically reduced, allowing the felsic melt to back-vein the mafic magma. The influx of felsic melt results in breakdown of hydrous minerals (i.e., amphibole and biotite) in the mafic system resulting in liquids of titanite composition. These liquids get incorporated into the incoming felsic melt as an immiscible phase and flow with it. The felsic melt and the immiscible titanite-liquid, both occupy the void spaces left behind by escaping gases/volatiles in the mafic system ultimately forming rounded titanite ocelli.

Keywords: titanite liquid; rheological contrast; thermal equilibrium; element diffusion; back-vein; Chotanagpur Granite Gneiss Complex.

INTRODUCTION

Many granitic magma chambers are often intruded by mantle-derived mafic magmas leading to mixing and mingling processes. Such interactions of disparate magmas are known to occur in both plutonic and volcanic systems. However, the complex process of magma mixing can be better traced in slowly cooled plutonic rocks than in the rapidly cooled volcanic ones. Direct evidence of magma interaction is given by outcrop level magmatic structures like mafic synplutonic dykes, mafic sheets and mafic magmatic enclaves (MME) within felsic host (Didier and Barbarin, 1991). However, these structures may also occur in other petrogenetic scenarios like a) xenoliths, fragments of older country rocks (Didier and Barbarin, 1991) b) autoliths or cognate xenoliths, older fragments derived from the host itself (Noyes et al., 1983; Chappell et al., 1987; Dahlquist, 2002; Ilbeyli and Pearce, 2005) c) restite, residual from the partial melting of the source rocks (White and Chappell, 1977). Geochemical signatures play the most vital role in distinguishing the occurrence of magma mixing from the other scenarios.

Rectilinear compositional trends on bivariate plots and hyperbolic compositional trends on ratio-ratio plots are considered as reliable parameters to recognize hybrid rocks that have formed from the advanced blending of two compositionally distinct magmas (Johnston and Wyllie, 1988; Neves and Vauchez, 1995; Tate et al., 1997). Although rectilinear trends on bivariate plots strongly suggest magma mixing, linear arrays on binary diagrams can also be a result of crystal fractionation and

accumulation, assimilation of non-restitic solids and restite unmixing (De Paolo, 1981; Chappell et al., 1987; Wall et al., 1987; Albarède, 1995; Janoušek et al., 2004). Even radiogenic isotopes may sometimes fail to provide evidence for magma mixing where there is limited isotopic contrast between the putative end-members. In such a scenario the hybrid masses and enclaves may undergo chemical exchange with the host magma and attain complete chemical equilibrium with the latter (Pin et al., 1990; Holden et al., 1991; Elburg, 1996; Waight et al., 2000, Janoušek et al., 2004). Thus, it is not a full proof approach to assess magma mixing based merely on geochemical parameters. More robust evidence can be offered by detailed mineral chemistry of the phases involved in disequilibrium textures preserved during magma mixing, and complimentary to bulk rock data (Vernon, 1990, 1991; Hibbard, 1991, 1995; Elburg et al., 1995). In mineral chemistry, plagioclase is considered to be an important mineral, particularly owing to the fact that plagioclase does not equilibrate during mafic-felsic magma interactions (Tepper and Kuehner, 2004) and may preserve valuable information about the processes governing magma mixing (Pietranik and Koepke, 2009).

The titanite-centered ocellar texture is a unique magma mixing feature formed under particular conditions (Hibbard, 1991). It is characterized by leucocratic ocelli of titanite enclosed in a biotite/hornblende-rich matrix. The ocelli consist of plagioclase, K-feldspar and quartz with titanite crystals at its centre. The study of this texture can reveal the mechanisms which ensue when two magmas come in contact and interact to attain equilibrium. Existing studies attributed the origin of this texture to different processes. Gelman (1962) suggested origin due to immiscibility phenomena. Processes like granitization of almost-crystallized mafic rocks by net-veined felsic material (Windley, 1965), destabilization of biotite during magma hybridization (Cuesta, 1991) and autometasomatism (Costa-de-Moura et al., 1997) have been also documented. Hibbard (1991) attributed the formation of this texture to a complex two-stage mixing model. Vegas et al. (2011) have suggested that the titanite-centered ocellar texture is evidence for grain-supported flow at low melt percentages and effect of dilatancy in a magma mush. Therefore, the exact mechanism by which titanite-centered ocellar texture forms is still debated. This work elucidates how this texture develops due to filling of vesicles by newly incorporated felsic melt in volatile-rich mafic magma based on petrographic and mineral-chemical evidences. As the exact processes by which mixing occurs are unclear, this type of disequilibrium texture can help to understand the mechanisms facilitating magma mixing and magma chamber dynamics involving two distinct magmas.

GEOLOGIC SETTING AND FIELD RELATIONS

The titanite ocelli occurring in the hybrid rock of the Nimchak Granite Pluton (NGP) have been studied in the present work. The NGP is part of the Bathani volcano-sedimentary sequence (BVSs) located on the northern fringe of the Chotanagpur Granite Gneiss Complex (CGGC) (Figure 1 a,b). The CGGC is a Proterozoic high-grade metamorphic terrain in the eastern part of the Central India Tectonic Zone (CITZ) covering about 80000 km^2. The terrain is bounded by two low grade mobile belts, namely the North Singhbhum Mobile Belt (NSMB) in the south and the Mahakoshal Mobile Belt (MMB) in the north. The BVSs is the eastern extension of MMB associated with CGGC (Saikia et al., 2014).

The Nimchak Pluton is about 1 km^2 granite magmatic pluton that was intruded by a number of mafic dykes causing mixing and mingling of magmas (Figure 1c). A total of about eight small to large mafic dykes (the smallest and the largest dykes show a thickness of around 5 m and 150 m, respectively) intruded the granitic magma chamber during the whole crystallization history of the chamber. Two varieties of granites are observed in the pluton; a coarse grained type occurring at the base of the pluton and a fine grained type placed towards the top (Figure 2 a,b). Probably the pluton exhibits a zoned magma chamber where fractional crystallization caused the zonation. The intrusion of mafic magma commenced when the felsic magma was partly crystallized (i.e., the base of the chamber was occupied by crystal mush) and continued till the whole chamber crystallized/solidified as indicated by the presence of two late stage mafic dykes (Figure 2c).

From field relationships it appears that mafic magma intruded the felsic magma chamber from its bottom and ascended through the lower crystal mush as restricted dykes. The upper part of the chamber was then occupied by a crystal poor liquid as indicated by the presence of abundant MME (mafic magmatic enclaves) toward the top. However, two dykes have been identified in the field, being continuous and cross-cutting the entire granitic pluton (i.e., both the upper and the lower granites). From field observations, it is quite evident that the two dykes are late-stage intrusions developing towards the end of the crystallizing granitic magma chamber. As these dykes were not involved in the mixing and mingling scenario, they are considered as representative of the parental mafic magma composition. The titanite ocelli occur in abundance within the zone of interaction between an earlier emplaced dyke and the granitic host (Figure 2 d,e).

PETROGRAPHY

The rocks of the NGP have been classified into three groups: 1) gabbros, represented by late stage mafic dykes which have not interacted with the granitic host and have

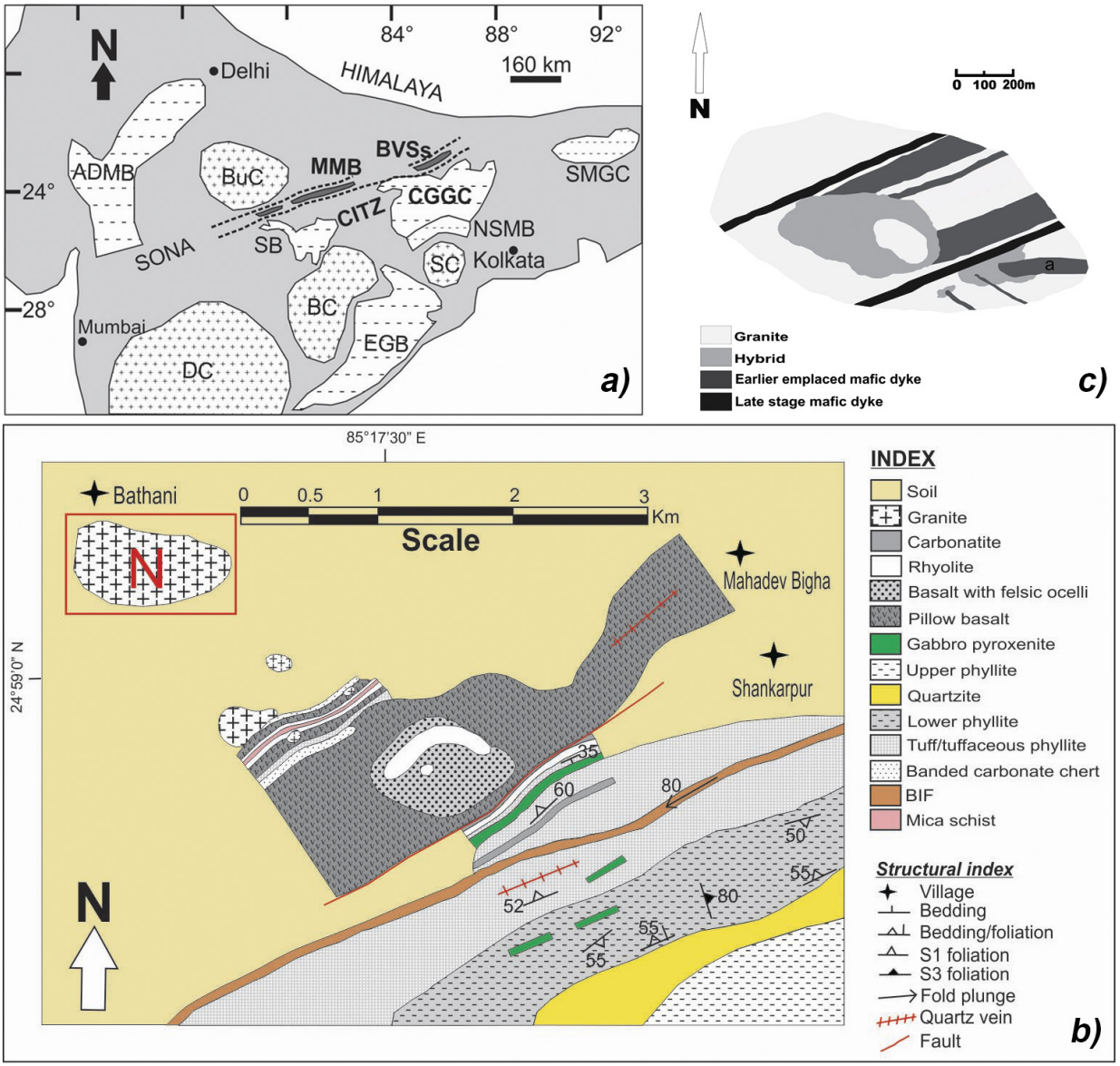

Figure 1. a) Location of Central India Tectonic Zone (CITZ) along with other Proterozoic mobile belts of India including Eastern Ghats Belt (EGB), Shillong Meghalaya Gneissic Complex (SMGC) and Aravalli Delhi Mobile Belt (ADMB). The CITZ comprises of Chotanagpur Granite Gneiss Complex (CGGC), Satpura Belt (SB), Mahakoshal Mobile Belt (MMB), North Singhbhum Mobile Belt (NSMB) and Bathani volcano-sedimentary sequence (BVSs). The MMB and BVSs lies within the ENE-WSW trending Son-Narmada (SONA) lineaments shown in dashed lines. Four Archean cratonic nuclei of India, namely Singhbhum (SC), Bastar (BC), Bundelkhand (BuC) and Dharwar (DC) are also shown (modified after Chatterjee and Ghose, 2011); b) Detailed geological map of the BVSs showing the location of the Nimchak Granite Pluton (NGP) marked as N (modified after Ahmad and Dubey, 2011 unpublished manuscript; Ahmad and Paul, 2012); c) Simplified geological map of the Nimchak Granite Pluton (NGP) showing the occurrence of eight mafic dykes and hybrid rocks in granite. The hybrid rocks have formed due to the interaction between mafic and felsic magmas. Two late-stage mafic dykes occurring in the pluton that have not interacted with the host granitic magma are also shown.

retained their original chemistry, 2) granites, representing the felsic magma, and 3) diorites (hybrid rocks) containing titanite ocelli which formed from the mixing and mingling of felsic and mafic components.

Late stage mafic dyke

The rocks exhibit holocrystalline textures consisting of augite, plagioclase, Ti-Fe oxide as major phases together with amphibole, chlorite, biotite, epidote, calcite as

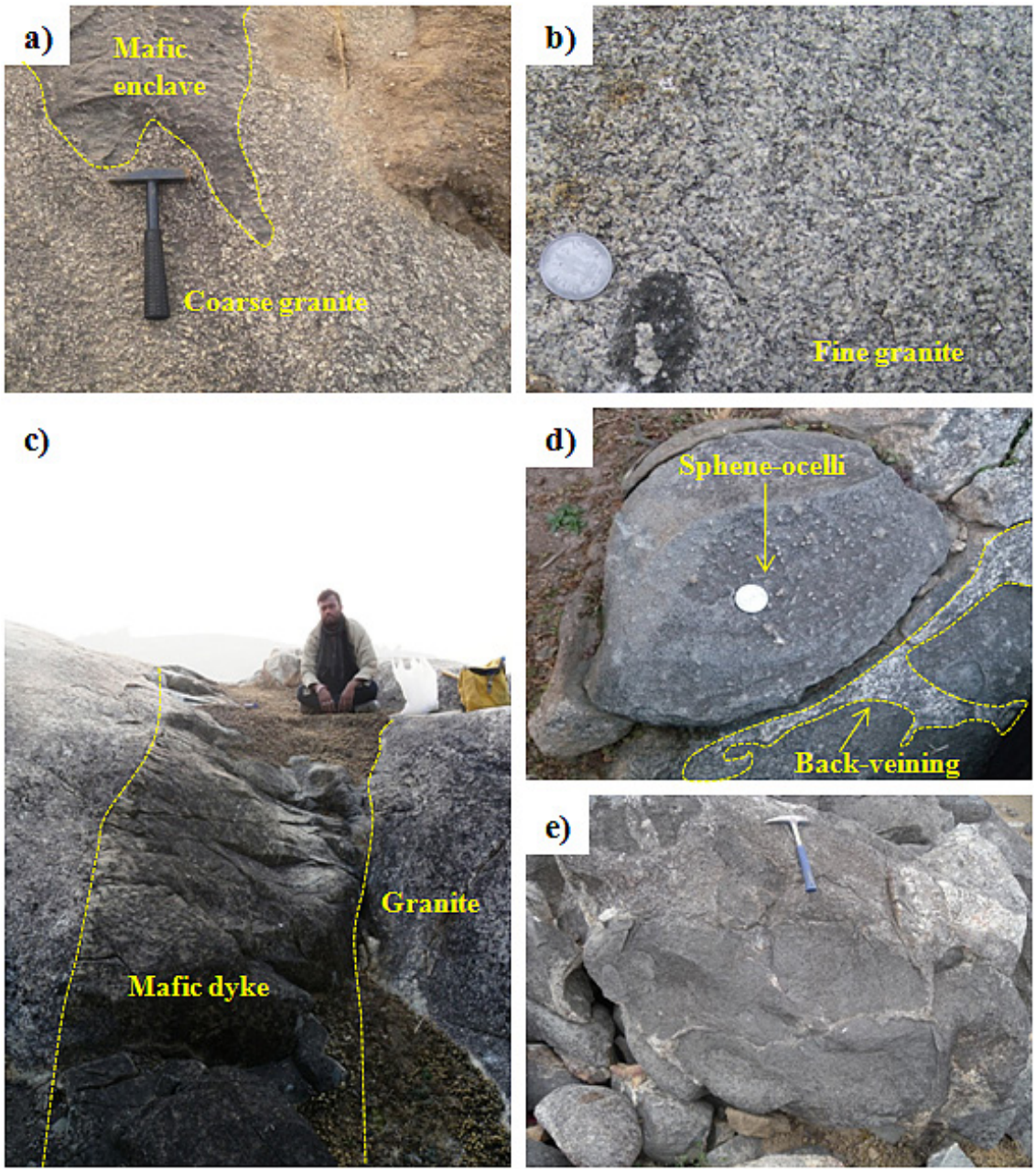

Figure 2. Field photographs displaying a) Coarse granite in association with a mafic magmatic enclave (MME) which is present towards the base of the pluton b) Finer granite containing a small MME occurring towards the top of the pluton c) A late-stage mafic dyke in granite d) Hybrid rock displaying titanite-centered ocellar texture. Granite back-veining can also be seen in the rock e) Interaction zone between an earlier emplaced mafic dyke and host granite where titanite ocelli occur in abundance.

accessory phases. Phenocrysts of augite embedded in the matrix gives the rock a porphyritic texture. Most of the plagioclase laths are partially or completely impinged within augite grains characterizing sub-ophitic and ophitic texture. Abundant vesicles are observed filled with secondary minerals like chlorite and calcite (Figure 3a).

Granite

The granite is fine to coarse grained with mineral grains of subhedral and anhedral shape. The rocks consist of biotite, quartz, feldspars as major phases and muscovite, chlorite, epidote, apatite, titanite, sericite, zircon, monazite, allanite and iron-oxide as accessory phases. Myrmekitic intergrowth of plagioclase and

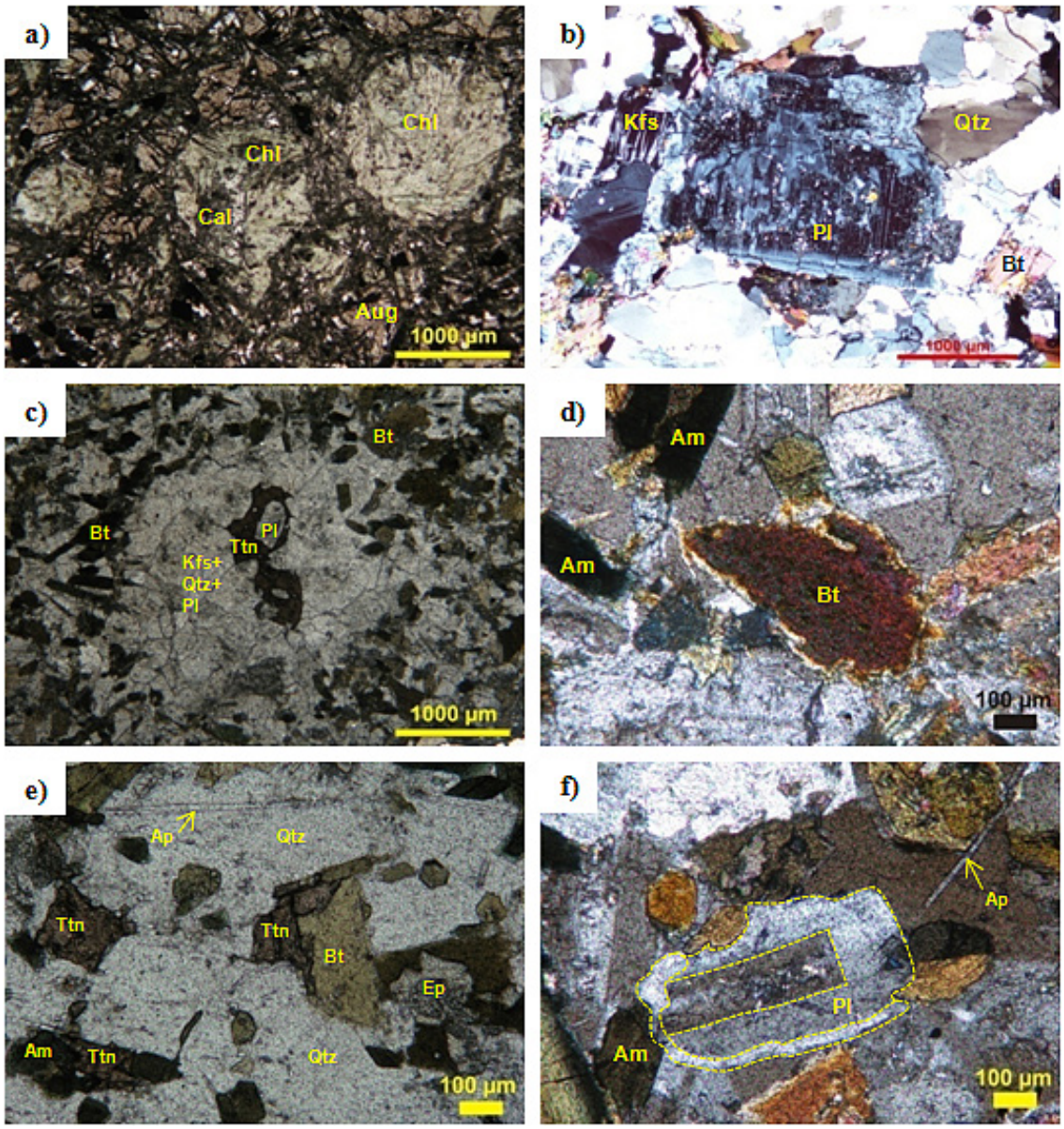

Figure 3. Photomicrographs displaying a) Vesicles in late-stage mafic dyke filled with secondary minerals like chlorite and calcite. The matrix consists of augite, plagioclase and Ti-Fe oxide. b) Plagioclase in finer granite displaying boxy-cellular morphology. c) Spherical titanite ocelli in hybrid rock. d) Resorbed biotite in hybrid rock. e) Biotite and amphibole getting altered to epidote and titanite. Acicular apatite is visible at the upper-end of the photomicrograph. These minerals appear to be embedded within anhedral masses of quartz. f) Plagioclase in the hybrid rock showing three compositional zonations. Mineral abbreviations: Am=amphibole, Ap=apatite, Aug=augite, bt=biotite, Cal=calcite, Chl=chlorite, Ep=epidote, Kfs=K-feldspar, Pl=plagioclase, Qtz=quartz, Ttn=titanite.

quartz is commonly observed. Micrographic intergrowth of quartz in K-feldspar can also be found. Perthitic and mesoperthitic exsolution lamellae of plagioclase feldspar in orthoclase and microcline are observed in the granites. Anti-perthitic texture has been also observed in some rocks. Compositional zoning and boxy-cellular morphology have been found for some plagioclases (Figure 3b).

Hybrid rock

The hybrid rock with titanite ocelli essentially contains amphibole, biotite, plagioclase, epidote, quartz, titanite, K-feldspar (orthoclase and microcline) and apatite. The titanite-centered ocellar texture is characterized by leucocratic ocelli of plagioclase, K-feldspar and quartz with titanite crystals at the centre enclosed in a biotite/hornblende-rich matrix (Figure 3c).

Amphibole and biotite display resorption features indicative of disequilibrium crystallization (Figure 3d). Some grains of these two minerals are altered to epidote and titanite (Figure 3e). Apatite mostly shows acicular habit in thin section (Figure 3 e,f). Most of the plagioclase grains are zoned with distinct rim and core (Figure 3f). Resorption texture is also common in plagioclase. Quartz and K-feldspar commonly occur as large anhedral crystals including smaller grains of other mineral phases present (Figure 3e). K-feldspar shows prominent perthitic exsolution texture.

The ocelli are mainly composed of anhedral masses of perthitic K-feldspar and quartz along with well developed grains of plagioclase, titanite and acicular apatite. The titanite crystals generally occur at the centre of ocelli, commonly in ophitic relationship with plagioclase laths.

ANALYTICAL METHODS

Mineral-chemical analyses were performed using a CAMECA SX 100 electron microprobe at Electron Microprobe Analyzer Laboratory, Geological Survey of India, Faridabad (India). The data were obtained using an acceleration voltage of 15 kV, beam current of 10 nA and a beam diameter of ca. 1 μm. Standards used includes Wollastonite for Si and Ca, Periclase for Mg, Rhodonite for Mn, Albite for Na, Corundum for Al, Hematite for Fe, Orthoclase for K, Apatite for P, metallic Cr and Ti for Cr and Ti, Halite for Cl, Metallic Zn for Zn, Fluorite for F and Barite for Ba. The correction applied to the data is that of PAP (Pouchou and Pichoir, 1987).

Analysis of major oxides and trace elements were carried out using the X-ray fluorescence (XRF) spectrometry (Bruker S8 Tiger Sequential X-ray Spectrometer with Rh excitation source) following the procedure of Saini et al., (1998, 2000) and rare earth elements (REE) were analysed using inductively coupled plasma mass spectrometry (ICP-MS) (Perkin Elmer made SCIEX quadrapole type ICP-MS, ELAN DRC-e), at the Wadia Institute of Himalayan Geology, Dehradun (India). For the major oxides, the operating conditions were: No filter, Vacuum path, 20/40KV. For trace elements the operating conditions were: No filter, Vacuum path, 55/60KV. The overall accuracy in relative standard deviation percentage is <5% for major and minor oxides and <12% for the trace elements. The average precision is better than 2% (Saini et al., 2007; Purohit et al., 2006). Sample solutions were introduced for rare earth element analysis into the argon plasma using a peristaltic pump and a cross flow nebulizer. The procedures adopted for sample digestion and preparation of solutions were that of Balaram et al. (1990). USGS (BHVO-1, AGV-1) and JGS (JG-2, RGM-1) samples were used as rock standards to minimize matrix effect. Relative standard deviation (RSD) for most of the samples is better than 10%.

MINERAL CHEMISTRY

Mineral-chemical analyses were determined from the different rock types of the study area, i.e., late-stage mafic dykes, granite and titanite ocelli bearing hybrid rock. Mineral chemistry has been used to trace the genesis of the hybrid rock that led to the formation of the unique titanite-centered ocellar texture (Figure 4; Middlemost, 1994).

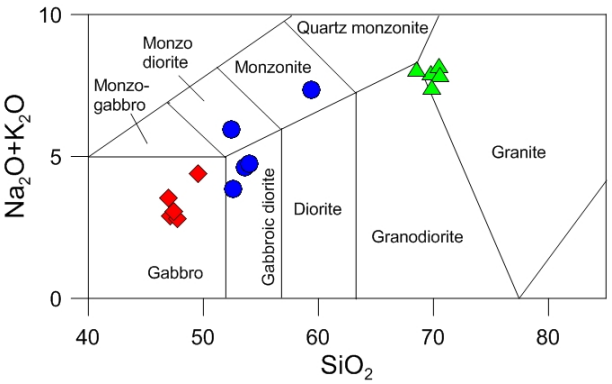

Figure 4. Total alkali vs. silica plot (Middlemost, 1994) showing the geochemical nomenclature of the studied rocks. Symbols represent: solid diamond=late-stage mafic dykes, solid triangle: felsic rocks, solid circle=hybrid rocks.

Pyroxene

Pyroxene is found exclusively in the mafic end-member from NGP. The end-member calculation of pyroxene has been done on the basis of six oxygen atoms (Morimoto et al., 1988) and ferric and ferrous iron values have been calculated according to Droop (1987). Representative analyses of pyroxene which include core-rim data from individual grains are reported in Table 1. The mineral is classified as Ca-Mg-Fe clinopyroxene and plots in the augite field (Figure 5) based on the classification of Morimoto et al. (1988). It is observed that a few clinopyroxene crystals are unzoned and when zoned the crystals show both magnesian-rich and magnesian-poor cores relative to rims (Table 1).

Feldspar

The data of plagioclase occurring in the mafic end-member of NGP, which include core-rim analyses of plagioclase grains, are given in Table 2. The analysed plagioclase grains are labradorite in composition (Figure 6a) and show normal zoning with more anorthitic cores relative to rims.

The representative data of plagioclase from the felsic end-member are provided in Table 3. The plagioclase compositions plot in the fields of oligoclase and andesine (Figure 6b). Analyses have been also carried out on

Table 1. Representative electron microprobe analyses of pyroxene in wt% oxide from the mafic end-member.

	Grain 1		Grain 2		Grain 3		Grain 4		Grain 5		Grain 6	
Location	Core	Rim	Core	Rim	Core	Rim	Core	Rim	Core	Rim	Core	Rim
SiO_2	46.75	49.72	49.51	50.36	48.88	48.85	50.95	50.42	49.68	49.89	50.86	49.37
TiO_2	0.96	1.29	1.42	0.85	1.65	1.46	0.83	1.08	0.97	1.08	0.95	1.39
Al_2O_3	8.00	2.55	2.55	2.02	3.62	3.38	2.04	1.90	1.53	2.07	2.08	3.62
FeO	11.50	11.48	12.05	12.14	11.55	11.39	11.78	11.82	12.88	13.91	10.79	10.80
MnO	0.34	0.30	0.24	0.27	0.27	0.28	0.37	0.29	0.36	0.36	0.31	0.24
MgO	13.00	12.96	12.79	13.12	12.61	12.95	14.11	14.60	13.34	11.50	14.30	13.47
CaO	17.63	18.94	19.42	18.73	20.07	19.90	18.25	18.10	18.98	19.84	19.22	19.97
Na_2O	0.27	0.39	0.35	0.35	0.34	0.39	0.24	0.29	0.29	0.34	0.30	0.36
K_2O	0.00	0.02	0.00	0.01	0.00	0.00	0.02	0.00	0.00	0.00	0.01	0.00
BaO	0.00	0.17	0.00	0.00	0.00	0.06	0.12	0.09	0.00	0.00	0.07	0.00
Total	98.45	97.82	98.32	97.85	98.99	98.65	98.71	98.57	98.01	98.98	98.86	99.22
Calculation based on six oxygens												
Si	1.78	1.91	1.90	1.93	1.86	1.87	1.94	1.92	1.92	1.92	1.92	1.87
Al^{IV}	0.22	0.09	0.10	0.07	0.14	0.13	0.06	0.08	0.07	0.08	0.08	0.13
Al^{VI}	0.14	0.03	0.02	0.02	0.03	0.02	0.03	0.01	0.00	0.02	0.01	0.03
Ti	0.03	0.04	0.04	0.02	0.05	0.04	0.02	0.03	0.03	0.03	0.03	0.04
Fe^{3+}	0.07	0.02	0.03	0.03	0.06	0.08	0.01	0.04	0.08	0.04	0.05	0.07
Fe^{2+}	0.30	0.35	0.35	0.36	0.31	0.29	0.37	0.33	0.34	0.41	0.29	0.28
Mg	0.74	0.74	0.73	0.75	0.72	0.74	0.80	0.83	0.77	0.66	0.81	0.76
Mn	0.01	0.01	0.01	0.01	0.01	0.01	0.01	0.01	0.01	0.01	0.01	0.01
Na	0.02	0.03	0.03	0.03	0.03	0.03	0.02	0.02	0.02	0.03	0.02	0.03
Ca	0.72	0.78	0.80	0.77	0.82	0.82	0.74	0.74	0.79	0.82	0.78	0.81
Total	4.02	4.00	4.01	3.99	4.01	4.02	4.00	4.01	4.02	4.01	4.00	4.02
Q	1.76	1.87	1.88	1.88	1.84	1.84	1.91	1.90	1.89	1.89	1.88	1.85
J	0.04	0.06	0.05	0.05	0.05	0.06	0.04	0.04	0.04	0.05	0.04	0.05
Wo (%)	39.21	41.02	41.49	40.14	42.85	42.31	38.53	37.81	39.64	42.23	40.23	42.19
Di (%)	40.22	39.07	38.02	39.10	37.45	38.31	41.43	42.43	38.77	34.06	41.64	39.60
Fe (%)	20.57	19.92	20.50	20.76	19.70	19.38	20.04	19.76	21.59	23.71	18.14	18.21
Mg#	71.10	68.20	67.48	67.61	70.05	71.94	68.59	71.41	69.47	61.76	73.37	73.31

Q=Ca+Mg+Fe^{2+}, J=2*Na, Wo=Wollastonite, Di=Diopside.

perthitic feldspars which include the host alkali feldspar and exsolution lamellae. The compositions of the host alkali feldspar are mostly orthoclase (Or_{94-96}) and that of exsolution lamellae is albite (Ab_{94-95}) (See Table 3).

Plagioclase occurring in the hybrid rock sample has been classified into four groups: a) plagioclase occurring in ophitic relationship with titanite in the ocelli b) those which are present in the ocelli but not in ophitic relationship with titanite c) those which are present as exsolution lamellae in K-feldspar in the ocelli, and d) plagioclases which are present in the matrix outside the ocelli. The chemical analyses are listed in Table 4. Most of the plagioclase grains occurring in the ocelli (i.e., plagioclase occurring as inclusion in titanite and those which are present in the ocelli but not in ophitic relationship with titanite) are compositionally zoned (Figure 6 c,d). The plagioclase occurring as inclusion in titanite has a labradorite core (An_{67}) with an intermediate zone of andesine composition (An_{35-37}). However, a few grains are dominantly andesine and lack the labradorite core. The plagioclase occurring in the ocelli is also generally characterized by a labradorite core (An_{67}) having an outer andesine composition (An_{35-37}) with a distinct albitic rim (An_{94}) clearly visible in backscattered image (Figure 7).

The plagioclase occurring as exsolution lamellae in

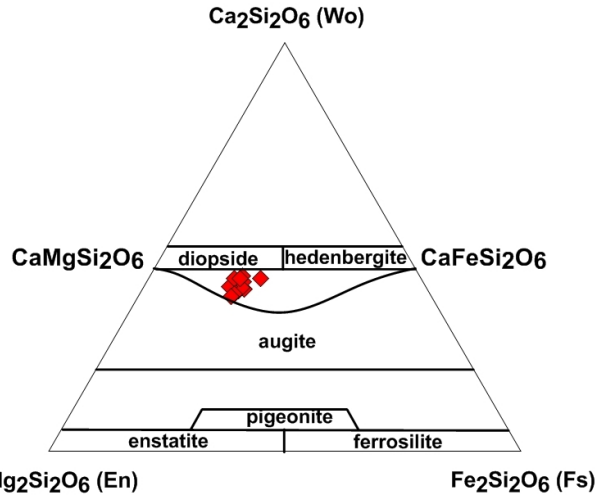

Figure 5. $Fe_2Si_2O_6$-$Mg_2Si_2O_6$-$Ca_2Si_2O_6$ diagram (Morimoto et al., 1988) showing the composition of pyroxenes from the mafic end-member.

K-feldspar (Or_{95}) is purely albitic (Ab_{97-98}) (Figure 6e). Plagioclase occurring in the matrix of the hybrid rock also shows crystal zoning (Figure 6f). At least three distinct compositional zones have been identified through plagioclase chemistry. The most calcic zone is labradorite (An_{55}), which occupies the core of the plagioclase grains. However, this zone is not present in all the grains. The more calcic labradorite zone, when present, is surrounded by an andesine zone. The andesine zone is present in all the plagioclase grains. Sometimes, the whole grain, from core to rim, may be of andesine composition grading into oligoclase towards the rim (An_{26-39}). Finally, a thin film of albite (Ab_{98}) has been found to surround many plagioclase grains. K-feldspar occurring in the ocelli shows perthitic texture, clearly visible in the back-scattered image (Figure 7). The composition of K-feldspar (Or_{95}) is given in Table 4.

Amphibole

Amphibole occurs as a major phase exclusively in the hybrid rock. It is classified as Ca-amphibole based on classification of Leake et al. (1997). The amphibole compositions plot in the fields of hastingsite, ferropargasite, ferrotshermakite and ferrohornblende (Figure 8 a,b). The Si content in amphibole varies from 5.98 to 6.57 a.p.f.u. (atom per formula unit) whereas Mg# varies from 0.34 to 0.49 (Table 5). Amphibole from the studied rock indicates an igneous origin. This is supported by the Si values of the amphibole which do not exceed the 7.50 a.p.f.u. limit for igneous amphibole (Leake, 1971). The igneous nature of the amphibole is clearly depicted by the calcic amphibole discrimination diagram of Fleet and Barnett (1978) in which the amphibole distinctly plots in the igneous field (Figure 9).

Biotite

The representative data of biotite occurring in the mafic end-member of NGP are given in Table 6. The biotite mostly plots in the field of siderophyllite (Figure 10a) (Deer et al., 1980; Rieder et al., 1998). The Fe# of biotite ranges from 0.47 to 0.58 and is classified as Mg-biotite (Figure 10b) (Tischendorf, 1997).

Biotite occurring in the felsic end-member can be classified as Fe-biotite and siderophyllite (Figure 10 c,d). The Si value of biotite varies from 2.51 to 2.85 and total Al varies from 1.53 to 2.01. The Fe+Mg value of the Fe-biotite ranges from 2.18 to 2.56 (Table 7).

Representative analyses and calculated formula of biotite from the hybrid rock are presented in Table 8. Biotite shows composition with SiO_2=35.93-36.82 wt%, FeO=20.47-22.02 wt%, Al_2O_3=15.46-17.08 wt% and K_2O=8.7-9.32 wt% and can be classified as Mg-biotite and annite (Figure 10 e,f). The biotite occurring in the titanite-ocelli bearing hybrid rock belongs to a single population group having restricted compositional range.

Titanite

Titanite occurring in the hybrid rock has been classified into three groups: a) titanite crystals which occur at the core of the ocelli b) those which are present in the matrix c) those which are present as inclusions in biotite and amphibole. The compositions of titanite occurring in the matrix and as inclusions in biotite and amphibole are identical in terms of major element cation values (Table 9). However, titanite occurring at the core of the ocelli exhibit high values of Ti and Na and depleted values of Al and F in comparison to that of the titanite in matrix and as inclusions. Moreover, titanite in the ocelli shows patchy zoning which is not evident in the other two types (Figure 7).

WHOLE ROCK GEOCHEMISTRY

Bulk rock geochemical data of the different rock types from NGP (mafic, felsic and hybrid) have been done to confirm the occurrence of magma mixing by means of major oxide linear correlation test (Fourcade and Allégre, 1981). A total of 15 samples representing each of the three different rock types have been analyzed for major oxides, trace elements (i.e., Ba, Co, Cr, Cu, Ga, Nb, Ni, Pb, Rb, Sc, Sr, Th, U, V, Y, Zn, Zr) and rare earth elements (REE) (Table 10).

Mixing test

The hybrid rock containing titanite ocelli has formed due to the interaction of both felsic and mafic magmas. The linear correlation from major oxide mixing test of Fourcade and Allégre (1981) can be applied to estimate the relative contributions of both the end-member magmas in

Table 2. Representative electron microprobe analyses of plagioclase feldspar in wt% oxide from the mafic end-member.

	Grain 1		Grain 2		Grain 3		Grain 4		Grain 5		Grain 6		Grain 7		Grain 8	
Location	Core	Rim	Core	Rim	Core	Rim	Core	Rim	Core	Rim	Core	Rim	Core	Rim	Core	Rim
SiO_2	51.01	54.66	51.07	54.23	50.84	52.92	51.70	55.18	53.81	54.11	50.66	52.30	50.69	54.72	54.27	54.59
TiO_2	0.13	0.08	0.06	0.04	0.08	0.10	0.05	0.10	0.12	0.04	0.14	0.06	0.14	0.08	0.10	0.00
Al_2O_3	29.05	26.92	29.41	26.92	30.35	28.21	29.01	25.88	27.88	28.12	29.71	28.46	29.31	26.50	27.93	28.17
FeO	0.67	0.57	0.63	0.41	0.56	0.64	0.58	0.42	0.55	0.56	0.53	0.66	0.57	0.64	0.44	0.41
MnO	0.00	0.02	0.00	0.00	0.00	0.00	0.00	0.00	0.02	0.06	0.00	0.03	0.00	0.00	0.00	0.00
MgO	0.07	0.11	0.10	0.09	0.12	0.09	0.13	0.05	0.07	0.08	0.10	0.16	0.13	0.12	0.10	0.11
CaO	13.03	10.38	13.53	10.56	14.40	12.50	13.92	10.34	11.85	11.82	14.07	12.78	14.03	10.77	11.28	11.30
Na_2O	3.82	5.32	3.66	5.05	3.51	4.42	3.77	5.66	4.61	4.95	3.52	4.32	3.40	5.58	5.20	5.09
K_2O	0.12	0.21	0.24	0.29	0.16	0.31	0.24	0.45	0.32	0.32	0.16	0.21	0.15	0.28	0.19	0.42
BaO	0.00	0.08	0.16	0.00	0.00	0.12	0.12	0.14	0.00	0.14	0.00	0.00	0.00	0.09	0.00	0.08
Total	97.90	98.34	98.86	97.58	100.01	99.31	99.51	98.22	99.23	100.19	98.87	98.97	98.42	98.77	99.50	100.17
Calculation based on eight oxygens																
Si	2.37	2.51	2.36	2.49	2.32	2.42	2.37	2.53	2.46	2.45	2.34	2.39	2.35	2.51	2.47	2.47
Ti	0.00	0.00	0.00	0.00	0.00	0.00	0.00	0.00	0.00	0.00	0.00	0.00	0.00	0.00	0.00	0.00
Al	1.59	1.46	1.60	1.46	1.63	1.52	1.57	1.40	1.50	1.50	1.62	1.53	1.60	1.43	1.50	1.50
Fe	0.03	0.02	0.02	0.02	0.02	0.02	0.02	0.02	0.02	0.02	0.02	0.03	0.02	0.02	0.02	0.02
Mn	0.00	0.00	0.00	0.00	0.00	0.00	0.00	0.00	0.00	0.00	0.00	0.00	0.00	0.00	0.00	0.00
Mg	0.01	0.01	0.01	0.01	0.01	0.01	0.01	0.00	0.00	0.01	0.01	0.01	0.01	0.01	0.01	0.01
Ca	0.65	0.51	0.67	0.52	0.70	0.61	0.68	0.51	0.58	0.57	0.70	0.63	0.70	0.53	0.55	0.55
Na	0.34	0.47	0.33	0.45	0.31	0.39	0.34	0.50	0.41	0.43	0.32	0.38	0.31	0.50	0.46	0.45
K	0.01	0.01	0.01	0.02	0.01	0.02	0.01	0.03	0.02	0.02	0.01	0.01	0.01	0.02	0.01	0.02
Cl	0.00	0.00	0.00	0.00	0.00	0.00	0.00	0.00	0.00	0.00	0.00	0.00	0.00	0.00	0.00	0.00
F	0.01	0.00	0.00	0.04	0.01	0.01	0.00	0.02	0.00	0.03	0.00	0.04	0.00	0.00	0.00	0.00
Ba	0.00	0.00	0.00	0.00	0.00	0.00	0.00	0.00	0.00	0.00	0.00	0.00	0.00	0.00	0.00	0.00
Total	5.01	5.00	5.01	5.01	5.02	5.01	5.01	5.02	5.00	5.03	5.01	5.03	5.00	5.02	5.01	5.01
An (%)	64.86	51.24	66.22	52.69	68.78	59.89	66.19	48.97	57.58	55.83	68.22	61.31	68.90	50.80	53.92	53.79
Ab (%)	34.41	47.52	32.41	45.61	30.32	38.32	32.47	48.48	40.57	42.34	30.88	37.49	30.24	47.63	45.02	43.83
Or (%)	0.72	1.24	1.37	1.71	0.90	1.79	1.34	2.54	1.84	1.82	0.90	1.20	0.87	1.57	1.06	2.38

An=Anorthite, Ab=Albite, Or=Orthoclase

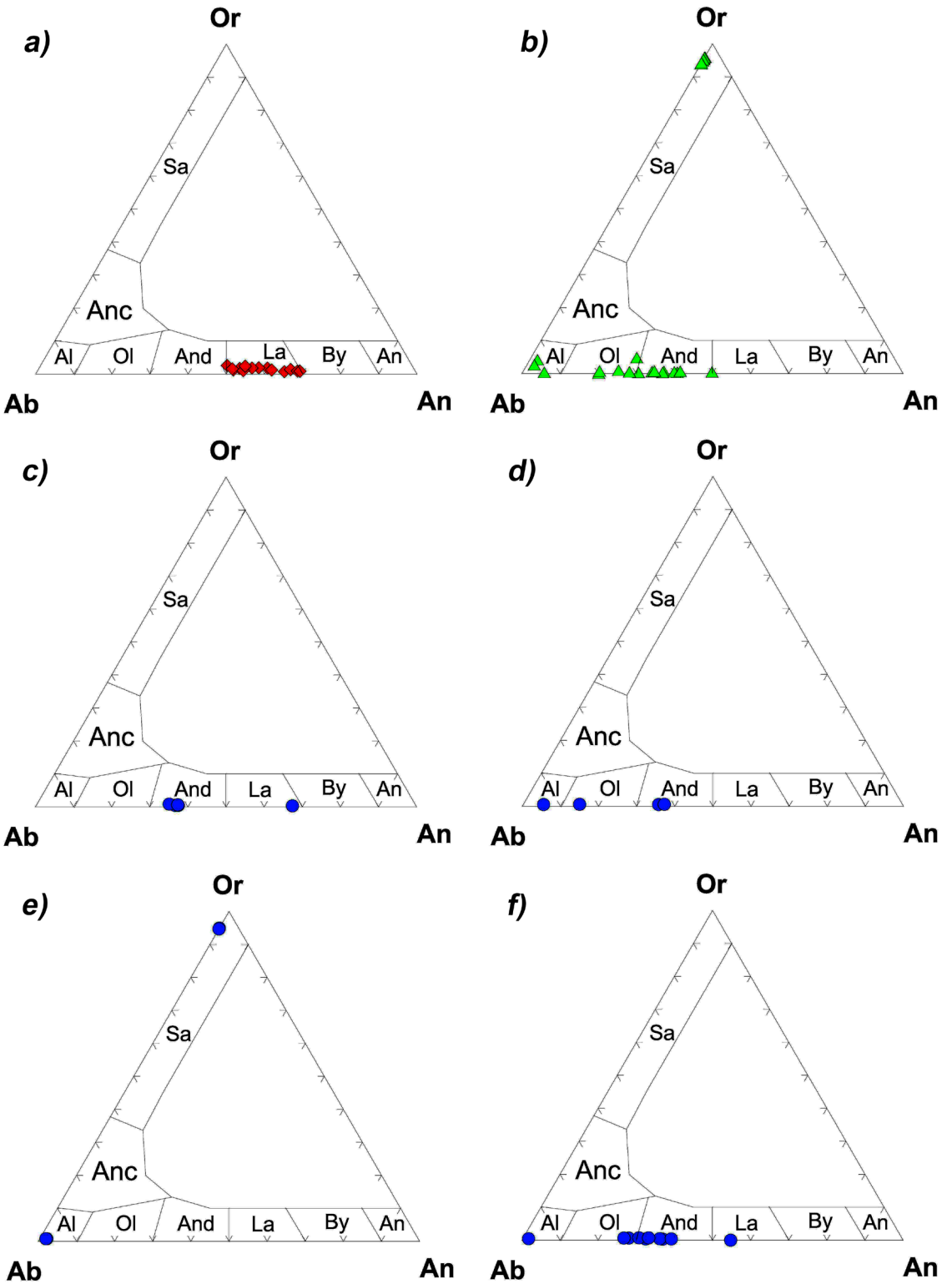

Figure 6. Nomenclature of feldspar occurring a) in the mafic end-member. b) in the felsic end-member. c) as inclusion in titanite in the ocelli of the hybrid rock. d) in the ocelli but not in ophitic relationship with titanite. e) as exsolution lamellae in K-feldspar within ocelli. The host K-feldspar is orthoclase. f) occurring in the matrix of the hybrid rock. Mineral abbreviations: An=anorthite, Ab=albite, Or=orthoclase, By=bytownite, La=labradorite, And=andesine, Ol=oligoclase, Anc=anorthoclase, Sa=sanidine.

Table 3. Representative electron microprobe analyses of feldspar in wt% oxide from the felsic end-member.

	Plagioclase feldspar													
SiO_2	59.05	58.25	59.05	59.87	58.13	56.24	63.59	59.63	57.33	58.65	63.83	59.57	57.49	60.93
TiO_2	0.00	0.00	0.05	0.04	0.00	0.00	0.00	0.06	0.02	0.00	0.06	0.12	0.00	0.10
Al_2O_3	25.16	25.39	25.20	25.67	25.73	27.22	22.47	23.83	25.97	25.08	22.32	25.04	30.33	24.48
FeO	0.15	0.03	0.00	0.20	0.05	0.06	0.00	0.22	0.06	0.03	0.07	0.00	0.13	0.01
MnO	0.03	0.00	0.00	0.03	0.00	0.00	0.00	0.02	0.00	0.00	0.00	0.00	0.04	0.02
MgO	0.00	0.00	0.00	0.15	0.00	0.00	0.00	0.00	0.00	0.00	0.00	0.01	0.05	0.00
CaO	7.65	8.27	7.54	5.65	8.29	10.27	4.24	7.30	8.63	7.14	4.18	6.43	4.82	6.00
Na_2O	7.15	6.65	7.13	7.58	6.89	5.71	9.32	7.82	6.74	7.45	9.16	8.09	7.96	8.50
K_2O	0.12	0.06	0.06	0.82	0.10	0.08	0.03	0.11	0.13	0.14	0.13	0.06	0.17	0.09
BaO	0.10	0.00	0.03	0.00	0.00	0.00	0.00	0.27	0.00	0.00	0.06	0.00	0.30	0.00
Total	99.40	98.65	99.05	100.00	99.18	99.58	99.65	99.26	98.87	98.50	99.81	99.32	101.30	100.12
Calculation based on eight oxygens														
Si	2.65	2.64	2.66	2.66	2.62	2.54	2.82	2.69	2.60	2.65	2.82	2.67	2.51	2.70
Ti	0.00	0.00	0.00	0.00	0.00	0.00	0.00	0.00	0.00	0.00	0.00	0.00	0.00	0.00
Al	1.33	1.35	1.34	1.35	1.37	1.45	1.17	1.27	1.39	1.34	1.16	1.32	1.56	1.28
Fe	0.01	0.00	0.00	0.01	0.00	0.00	0.00	0.01	0.00	0.00	0.00	0.00	0.00	0.00
Mn	0.00	0.00	0.00	0.00	0.00	0.00	0.00	0.00	0.00	0.00	0.00	0.00	0.00	0.00
Mg	0.00	0.00	0.00	0.01	0.00	0.00	0.00	0.00	0.00	0.00	0.00	0.00	0.00	0.00
Ca	0.37	0.40	0.36	0.27	0.40	0.50	0.20	0.35	0.42	0.35	0.20	0.31	0.23	0.29
Na	0.62	0.58	0.62	0.65	0.60	0.50	0.80	0.68	0.59	0.65	0.79	0.70	0.67	0.73
K	0.01	0.00	0.00	0.05	0.01	0.00	0.00	0.01	0.01	0.01	0.01	0.00	0.01	0.01
Cl	0.00	0.00	0.00	0.00	0.00	0.00	0.00	0.00	0.00	0.00	0.00	0.00	0.01	0.00
F	0.02	0.00	0.00	0.01	0.00	0.00	0.00	0.00	0.01	0.02	0.00	0.00	0.03	0.00
Ba	0.00	0.00	0.00	0.00	0.00	0.00	0.00	0.00	0.00	0.00	0.00	0.00	0.01	0.00
Total	5.00	4.98	4.98	5.01	5.00	4.99	5.00	5.02	5.01	5.01	4.99	5.02	5.05	5.02
An (%)	36.92	40.56	36.76	27.77	39.70	49.64	20.07	33.83	41.16	34.36	19.99	30.40	24.82	27.92
Ab (%)	62.42	59.06	62.89	67.44	59.76	49.93	79.77	65.58	58.12	64.84	79.26	69.26	74.14	71.57
Or (%)	0.66	0.37	0.34	4.79	0.55	0.43	0.16	0.59	0.72	0.80	0.75	0.33	1.04	0.51

An=Anorthite, Ab=Albite, Or=Orthoclase

Table 3. ...Continued

	Perthitic feldspar												
	Host K-feldspar										Exsolution		
SiO_2	63.11	63.73	64.17	64.36	64.04	64.35	64.37	63.76	64.18	64.14	68.40	69.04	66.73
TiO_2	0.00	0.04	0.00	0.05	0.02	0.00	0.00	0.03	0.00	0.00	0.00	0.00	0.04
Al_2O_3	18.35	18.56	18.20	18.30	18.08	18.19	18.58	18.62	18.54	18.58	19.62	19.56	21.21
FeO	0.00	0.06	0.03	0.00	0.02	0.00	0.00	0.00	0.00	0.01	0.00	0.04	0.00
MnO	0.00	0.01	0.00	0.03	0.06	0.00	0.07	0.02	0.04	0.00	0.00	0.00	0.00
MgO	0.01	0.00	0.00	0.02	0.00	0.00	0.00	0.00	0.03	0.02	0.00	0.00	0.00
CaO	0.00	0.00	0.00	0.00	0.01	0.04	0.00	0.00	0.00	0.00	0.44	0.41	1.21
Na_2O	0.57	0.44	0.50	0.52	0.50	0.44	0.47	0.50	0.64	0.59	11.29	11.10	11.08
K_2O	15.83	15.90	15.71	15.75	15.77	15.88	16.08	14.93	15.11	14.66	0.76	0.47	0.07
BaO	0.20	0.74	0.63	0.77	0.42	0.25	0.32	1.14	0.57	0.91	0.01	0.04	0.00
Total	98.06	99.48	99.25	99.80	98.91	99.15	99.89	99.01	99.12	98.90	100.51	100.66	100.34
Calculation based on eight oxygens													
Si	2.98	2.97	3.00	2.99	3.00	2.99	2.98	2.98	2.98	2.98	2.98	3.00	2.91
Ti	0.00	0.00	0.00	0.00	0.00	0.00	0.00	0.00	0.00	0.00	0.00	0.00	0.00
Al	1.02	1.02	1.00	1.00	1.00	0.99	1.02	1.02	1.02	1.02	1.01	1.00	1.09
Fe	0.00	0.00	0.00	0.00	0.00	0.00	0.00	0.00	0.00	0.00	0.00	0.00	0.00
Mn	0.00	0.00	0.00	0.00	0.00	0.00	0.00	0.00	0.00	0.00	0.00	0.00	0.00
Mg	0.00	0.00	0.00	0.00	0.00	0.00	0.00	0.00	0.00	0.00	0.00	0.00	0.00
Ca	0.00	0.00	0.00	0.00	0.00	0.00	0.00	0.00	0.00	0.00	0.02	0.02	0.06
Na	0.05	0.04	0.05	0.05	0.05	0.04	0.04	0.04	0.06	0.05	0.96	0.93	0.94
K	0.95	0.95	0.94	0.93	0.94	0.94	0.95	0.89	0.90	0.87	0.04	0.03	0.00
Cl	0.00	0.00	0.00	0.00	0.00	0.00	0.00	0.00	0.01	0.00	0.00	0.00	0.00
F	0.00	0.01	0.00	0.00	0.00	0.04	0.00	0.02	0.01	0.03	0.00	0.00	0.01
Ba	0.00	0.01	0.01	0.01	0.01	0.00	0.01	0.02	0.01	0.02	0.00	0.00	0.00
Total	5.01	5.01	4.99	5.00	4.99	5.00	5.00	4.98	4.98	4.97	5.01	4.98	5.01
An (%)	0.00	0.00	0.00	0.00	0.06	0.19	0.00	0.00	0.00	0.00	2.00	1.96	5.66
Ab (%)	5.18	4.04	4.60	4.77	4.56	4.00	4.25	4.81	6.08	5.78	93.86	95.40	93.93
Or (%)	94.82	95.96	95.40	95.23	95.39	95.82	95.75	95.19	93.92	94.22	4.14	2.64	0.41

An=Anorthite, Ab=Albite, Or=Orthoclase

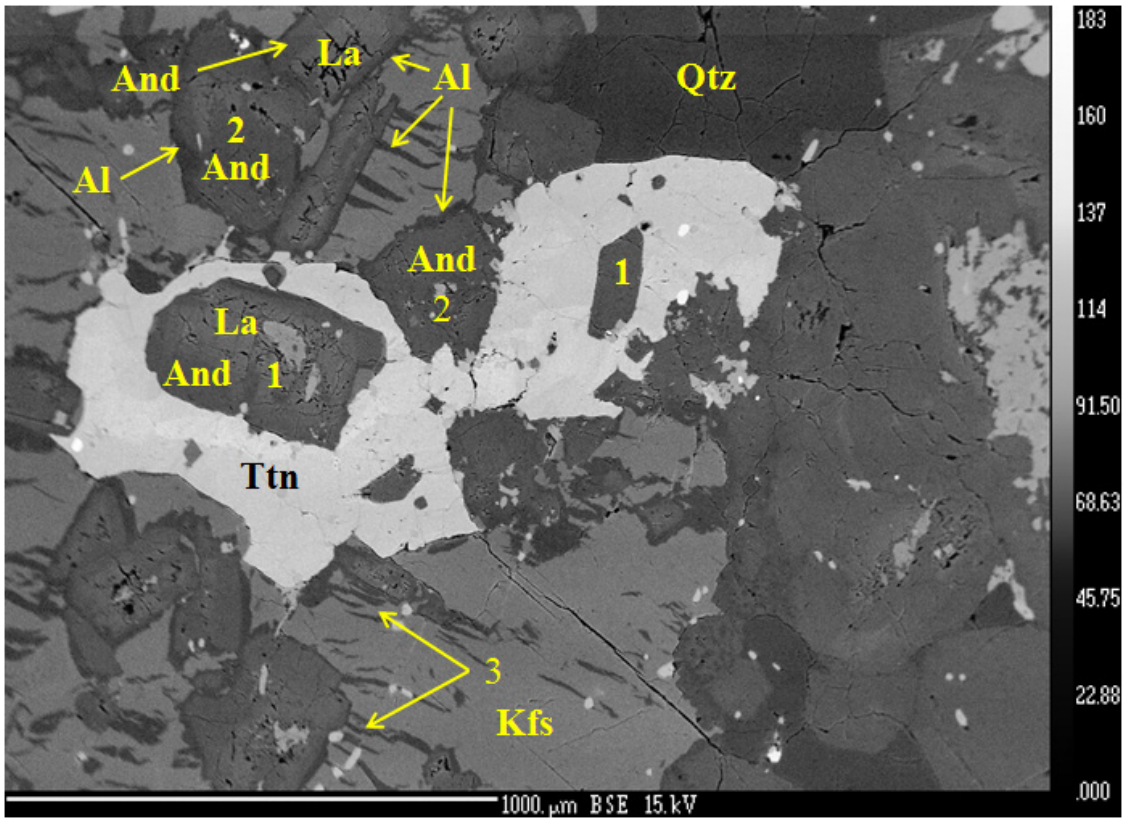

Figure 7. Back-scattered image of a titanite ocellus. Marked as 1 is plagioclase occurring as inclusion in titanite, marked as 2 plagioclase occurring in the ocelli but not as inclusion in titanite, as 3 plagioclase occurring as exsolution lamella in K-feldspar. Three compositional zones i.e., labradorite, andesine and albite can be identified in most of the plagioclase grains which are not present as inclusions in titanite. The plagioclase grains occurring as inclusions in titanite show distinct compositional behavior. The smaller grain is andesine in composition and lack zonations, while the larger grain exhibit distinct zonations with a labradorite core and an andesine rim. Mineral abbreviations: Al=albite, And=andesine, Kfs=K-feldspar, La=labradorite, Qtz=quartz, Ttn=titanite.

forming the hybrid rock. If mixing occurs, each element would be affected by the process as follows:

$$C^i_i - C^i_f = m\,(C^i_m - C^i_f)$$

where C^i_i is the concentration of i element in intermediate hybrid magma, C^i_f is the concentration of i element in felsic magma, C^i_m is the concentration of i element in mafic magma, and m is the fraction of mafic magma in the mixture. The plot of C^i_m-C^i_f versus C^i_i-C^i_f would result in a straight line whose slope gives the mass proportions of the mixture.

We have done the mixing test for two representative sample sets (Figure 11 a,b). The mixing test reveals good linear correlation for the titanite ocelli bearing hybrid rock with R^2>0.98. This sharp linearity observed for the hybrid rock may be attributed to a magma mixing scenario approaching complete homogenization. The slope obtained for the observed samples gives the fraction of mafic magma involved in the mixture. The fractions obtained for the hybrid rock is >70%.

PRESSURE-TEMPERATURE ESTIMATE

The crystallization temperatures and pressures of the mafic (gabbro), felsic (granite) and hybrid rock (diorite) from NGP were estimated using three distinct geothermometers and geobarometers. The crystallization temperature and pressure of the mafic end-member have been estimated using the clinopyroxene-only thermometer (Eq. 32d) and barometer (Eq. 32a) of Putirka et al. (2008b). Equation (32d) is a revised thermometer of Nimis and Taylor (2000), wherein a regression through 311 hydrous experiments had an R^2 value of 0.36 and an SEE of ±87 °C (Putirka 2008b). Equation (32a) is a revised barometer of Nimis (1995), wherein a regression through 854 anhydrous experiments had an R^2 value of 0.92 and an SEE of ±3.1 kbar (Putirka 2008b). The average crystallization temperature estimated for clinopyroxene

Table 4. Representative electron microprobe analyses of feldspar in wt% oxide from the hybrid rock displaying titanite-centered ocellar texture.

	In Ocelli												
	Inclusion in sphene					Not as inclusion in sphene				Exsolution		K-feldspar	
	Grain 1			Grain 2		Grain 3		Grain 4					
	Core	Intermediate	Rim	Core	Rim	Core	Rim	Core	Rim				
SiO_2	50.04	58.79	59.95	58.02	59.54	59.09	64.61	58.72	66.03	67.26	68.59	64.66	64.47
TiO_2	0.06	0.00	0.01	0.06	0.00	0.00	0.00	0.00	0.13	0.00	0.01	0.02	0.00
Al_2O_3	30.97	26.06	25.60	25.80	26.07	26.01	22.07	26.34	20.39	20.02	20.06	18.71	18.64
FeO	0.25	0.17	0.15	0.17	0.07	0.15	0.03	0.09	0.00	0.01	0.00	0.03	0.05
MnO	0.05	0.00	0.03	0.01	0.05	0.00	0.06	0.01	0.00	0.02	0.00	0.02	0.00
MgO	0.02	0.01	0.02	0.10	0.00	0.01	0.00	0.00	0.00	0.00	0.00	0.01	0.00
CaO	14.00	7.72	7.29	7.63	7.86	7.52	3.19	7.85	1.12	0.40	0.34	0.00	0.00
Na_2O	3.73	7.39	7.49	7.05	7.32	7.49	10.09	7.34	10.95	11.62	11.73	0.53	0.56
K_2O	0.06	0.08	0.14	0.08	0.11	0.09	0.10	0.10	0.10	0.14	0.15	15.19	15.18
BaO	0.00	0.00	0.00	0.27	0.00	0.00	0.00	0.23	0.00	0.11	0.00	0.73	0.07
Total	99.17	100.23	100.68	99.17	101.02	100.36	100.15	100.68	98.71	99.57	100.88	99.90	98.97
Calculation based on eight oxygens													
Si	2.30	2.62	2.66	2.62	2.63	2.62	2.85	2.61	2.93	2.96	2.97	2.99	2.99
Ti	0.00	0.00	0.00	0.00	0.00	0.00	0.00	0.00	0.00	0.00	0.00	0.00	0.00
Al	1.67	1.37	1.34	1.37	1.36	1.36	1.15	1.38	1.07	1.04	1.02	1.02	1.02
Fe	0.01	0.01	0.01	0.01	0.00	0.01	0.00	0.00	0.00	0.00	0.00	0.00	0.00
Mn	0.00	0.00	0.00	0.00	0.00	0.00	0.00	0.00	0.00	0.00	0.00	0.00	0.00
Mg	0.00	0.00	0.00	0.01	0.00	0.00	0.00	0.00	0.00	0.00	0.00	0.00	0.00
Ca	0.69	0.37	0.35	0.37	0.37	0.36	0.15	0.37	0.05	0.02	0.02	0.00	0.00
Na	0.33	0.64	0.64	0.62	0.63	0.64	0.86	0.63	0.94	0.99	0.99	0.05	0.05
K	0.00	0.00	0.01	0.00	0.01	0.01	0.01	0.01	0.01	0.01	0.01	0.90	0.90
Cl	0.00	0.00	0.00	0.00	0.00	0.00	0.00	0.00	0.00	0.00	0.00	0.00	0.00
F	0.02	0.00	0.00	0.01	0.01	0.02	0.00	0.00	0.01	0.01	0.01	0.01	0.00
Ba	0.00	0.00	0.00	0.00	0.00	0.00	0.00	0.00	0.00	0.00	0.00	0.01	0.00
Total	5.03	5.01	5.00	5.01	5.01	5.02	5.01	5.02	5.01	5.02	5.01	4.97	4.97
An (%)	67	36	35	37	37	35	15	37	5	2	2	0	0
Ab (%)	32	63	64	62	62	64	85	62	94	97	98	5	5
Or (%)	0	0	1	0	1	1	1	1	1	1	1	95	95

An=Anorthite, Ab=Albite, Or=Orthoclase

Table 4. ...Continued

	Matrix											
	Grain 5		Grain 6		Grain 7		Grain 8		Grain 9		Grain 10	
	Core	Rim	Core	Rim	Core	Rim	Core	Rim	Core	Rim	Core	Rim
SiO_2	58.94	67.51	58.48	60.91	58.49	57.91	54.49	60.45	61.13	62.85	58.93	60.74
TiO_2	0.00	0.07	0.04	0.15	0.01	0.00	0.00	0.00	0.00	0.00	0.00	0.00
Al_2O_3	25.79	19.98	25.58	25.05	25.42	26.58	28.11	24.87	24.43	24.63	26.03	25.08
FeO	0.03	0.02	0.06	0.17	0.04	0.05	0.06	0.04	0.05	0.06	0.19	0.28
MnO	0.00	0.02	0.10	0.00	0.00	0.00	0.00	0.00	0.05	0.02	0.03	0.06
MgO	0.01	0.00	0.00	0.06	0.00	0.00	0.00	0.00	0.01	0.00	0.02	0.00
CaO	7.53	0.33	7.64	5.89	7.45	7.58	11.17	6.91	6.24	5.64	8.06	6.86
Na_2O	7.32	11.51	7.33	8.41	7.05	7.42	5.10	7.95	7.84	8.60	6.92	7.65
K_2O	0.08	0.09	0.07	0.12	0.06	0.08	0.00	0.07	0.13	0.11	0.07	0.12
BaO	0.10	0.00	0.02	0.00	0.19	0.13	0.05	0.00	0.00	0.06	0.04	0.02
Total	99.80	99.51	99.31	100.77	98.71	99.74	98.99	100.28	99.88	101.97	100.27	100.81
Calculation based on eight oxygens												
Si	2.63	2.97	2.63	2.69	2.64	2.60	2.48	2.68	2.72	2.74	2.63	2.68
Ti	0.00	0.00	0.00	0.00	0.00	0.00	0.00	0.00	0.00	0.00	0.00	0.00
Al	1.36	1.03	1.36	1.30	1.35	1.40	1.51	1.30	1.28	1.26	1.37	1.31
Fe	0.00	0.00	0.00	0.01	0.00	0.00	0.00	0.00	0.00	0.00	0.01	0.01
Mn	0.00	0.00	0.00	0.00	0.00	0.00	0.00	0.00	0.00	0.00	0.00	0.00
Mg	0.00	0.00	0.00	0.00	0.00	0.00	0.00	0.00	0.00	0.00	0.00	0.00
Ca	0.36	0.02	0.37	0.28	0.36	0.36	0.54	0.33	0.30	0.26	0.38	0.33
Na	0.63	0.98	0.64	0.72	0.62	0.64	0.45	0.68	0.68	0.73	0.60	0.66
K	0.00	0.00	0.00	0.01	0.00	0.00	0.00	0.00	0.01	0.01	0.00	0.01
Cl	0.00	0.00	0.00	0.00	0.00	0.00	0.00	0.00	0.00	0.00	0.00	0.00
F	0.01	0.00	0.00	0.00	0.01	0.01	0.00	0.00	0.00	0.00	0.00	0.00
Ba	0.00	0.00	0.00	0.00	0.00	0.00	0.00	0.00	0.00	0.00	0.00	0.00
Total	5.01	5.01	5.01	5.02	4.99	5.03	4.99	5.01	4.98	5.00	4.99	4.99
An (%)	36	2	36	28	37	36	55	32	30	26	39	33
Ab (%)	63	98	63	72	63	64	45	67	69	73	61	66
Or (%)	0	0	0	1	0	0	0	0	1	1	0	1

An=Anorthite, Ab=Albite, Or=Orthoclase

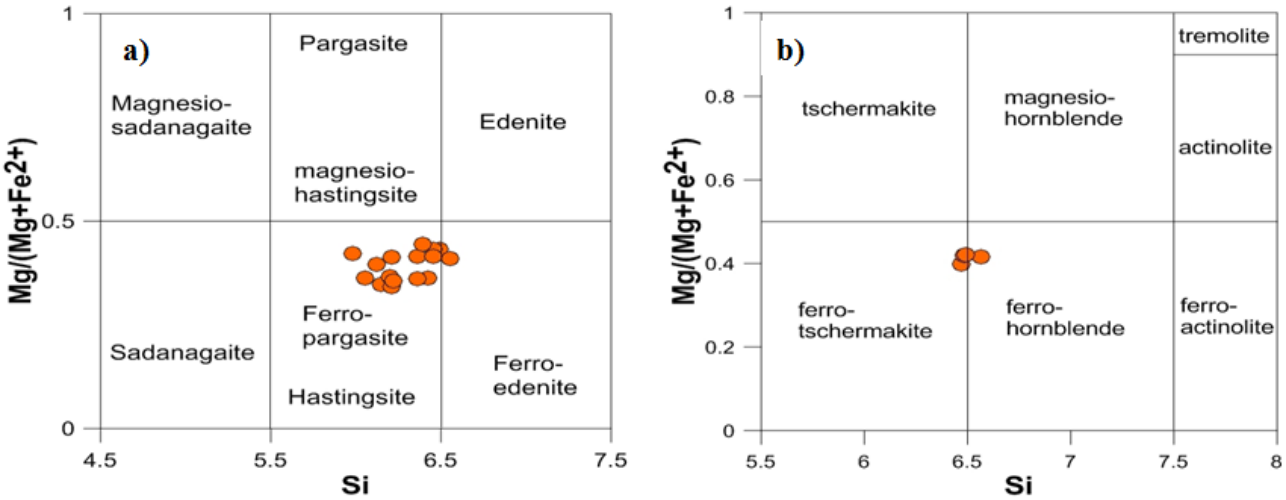

Figure 8. (a, b) Nomenclature of amphiboles occurring in the matrix of the hybrid rock displaying titanite ocelli (after Leake et al., 1997).

in mafic rocks is 1160 °C, while the estimated average pressure is 423 MPa (Supplementary Figure 1).

The igneous nature of the calcic amphibole allowed us to estimate temperature and pressure conditions of magma emplacement for the titanite ocelli bearing hybrid rock. Temperature was calculated using the hornblende-plagioclase equilibria thermometer (edenite-richterite thermometer) of Holland and Blundy (1994). Typical temperature uncertainty is stated as ±35-40 ºC for this thermometer. Mineral-chemical and petrographic observations show that the amphibole crystallized in equilibrium with the labradorite zones. Hence, labradorite composition in plagioclase has been used for temperature calculations. Pressure was calculated using the Al-in-hornblende barometer of Anderson and Smith (1995; P (±0.6kbar)={4.76AI-3.01-([T°(C)-675]/85}x{0.530AI+ 0.005294[T°(C)-675]}). Associated errors on the pressure estimates are ± 60 MPa. The pressures obtained for the hybrid rock varies from 176 to 609 MPa (average=373 MPa). The average pressure calculated from the Al-in-hornblende geobarometer corresponds to a depth of ca. 12 km. The temperatures of co-existing hornblende and plagioclase were calculated based on iteration using the pressure obtained from Al-in-hornblende barometer. The calculated equilibrium temperatures of co-existing hornblende and plagioclase are in the range of 763 ºC to 849 ºC (average=804 ºC) (Supplementary Table 1).

The magma temperature of the felsic end-member has been calculated from bulk rock compositions using the zircon saturation thermometry (Watson and Harrison, 1983; Miller et al., 2003).The thermometry established the following relationship among zircon solubility, temperature, and major element composition of melt:

$$\ln D^{Zr,\ zircon/melt}=\{-3.8-[0.85(M-1)]\}+12{,}900/T$$

where, $D^{Zr,zircon/melt}$ is the ratio of Zr concentration (ppm) in zircon (476,000 ppm) to that in the saturated melt; M is a compositional factor that accounts for dependence of zircon solubility on SiO_2 and peraluminosity of the melt [(Na+K+2*Ca)/(Al*Si), all in cation fraction]; and temperature, T, is in Kelvin. Rearranging the equation to yield T yields a geothermometer for melt:

$$T_{Zr}=12{,}900/[2.95+0.85M+\ln(496{,}000/Zr_{melt})]$$

This thermometer provides a good estimate of magma temperature during zircon crystallization. The uncertainity for the thermometer is ±24 °C (Miller et al., 2003). By using this thermometer, the temperatures obtained for the felsic end-member from NGP has a restricted range of 777 to 828 ºC with an arithmetic mean of 803 ºC (Supplementary Table 2).

DISCUSSION

Our study reveals that magma mixing in a plutonic environment occurs through a slow and gradual process through the interplay of a number of mechanisms. A detailed overview of the mechanisms is discussed below.

Attainment of thermal equilibrium

The NGP was a crystallizing granite magma chamber when mafic magma intruded it leading to magma mixing scenario. When mafic magma came in contact with its felsic counterpart, the first interaction that took place between the two magmas was diffusion of heat from the hotter mafic magma to the colder felsic magma. As

Table 5. Representative electron microprobe analyses of amphibole in wt% oxide from the hybrid rock displaying titanite-centered ocellar texture.

SiO_2	39.63	38.92	39.66	38.65	41.72	41.75	41.13	39.89	42.68	38.20	39.64	41.76	41.03	38.34	41.36	41.28	42.22	42.02	41.92	41.30	40.19
TiO_2	2.29	1.72	1.09	2.10	1.64	0.33	1.40	1.89	0.83	0.30	0.12	1.26	1.39	2.17	1.38	1.46	1.64	1.42	1.74	1.36	1.47
Al_2O_3	11.68	11.45	11.65	11.59	10.18	10.42	10.66	11.42	9.74	13.30	12.97	9.10	10.51	11.72	9.36	9.58	9.09	9.57	10.17	11.28	11.95
Cr_2O_3	0.01	0.03	0.04	0.00	0.00	0.00	0.01	0.00	0.00	0.00	0.00	0.00	0.00	0.00	0.00	0.02	0.00	0.00	0.00	0.01	0.00
FeO	22.39	22.70	22.44	22.56	21.74	22.21	22.38	23.61	21.96	23.33	23.26	22.09	22.11	22.82	21.52	22.09	21.78	21.88	21.21	22.62	23.10
MnO	0.79	0.55	0.64	0.81	0.63	0.52	0.75	0.74	0.71	0.69	0.54	0.77	0.70	0.80	0.81	0.72	0.59	0.78	0.60	0.65	0.73
MgO	6.67	5.81	6.72	5.71	7.02	7.14	6.28	5.78	7.33	6.26	5.75	7.55	7.11	5.97	7.60	7.66	7.40	7.39	7.48	6.34	5.92
CaO	11.53	11.31	10.79	11.27	11.40	11.65	11.47	11.45	11.79	10.92	11.12	11.64	11.42	11.59	11.65	11.55	11.65	11.67	11.71	11.80	11.72
Na_2O	1.23	1.11	0.95	1.13	1.01	1.06	0.95	1.07	1.02	1.41	1.24	1.07	0.99	1.22	1.20	1.07	1.07	0.94	1.12	1.07	0.98
K_2O	1.49	1.62	1.86	1.51	1.26	1.07	1.50	1.60	1.08	1.06	1.12	1.19	1.47	1.60	1.23	1.20	1.18	1.22	1.39	1.56	1.41
Total	97.70	95.22	95.83	95.32	96.60	96.15	96.51	97.43	97.15	95.46	95.76	96.43	96.73	96.23	96.11	96.62	96.62	96.88	97.33	97.99	97.47
Calculation based on twenty-three oxygens																					
Si	6.12	6.20	6.21	6.15	6.47	6.48	6.43	6.21	6.57	5.98	6.20	6.49	6.36	6.05	6.46	6.39	6.56	6.49	6.46	6.36	6.22
Al^{iv}	1.88	1.80	1.79	1.85	1.53	1.52	1.57	1.79	1.43	2.02	1.80	1.51	1.64	1.95	1.54	1.61	1.44	1.51	1.54	1.64	1.78
Sum T	8.00	8.00	8.00	8.00	8.00	8.00	8.00	8.00	8.00	8.00	8.00	8.00	8.00	8.00	8.00	8.00	8.00	8.00	8.00	8.00	8.00
Al^{vi}	0.25	0.35	0.36	0.32	0.33	0.39	0.39	0.31	0.33	0.44	0.59	0.16	0.28	0.24	0.18	0.14	0.22	0.24	0.30	0.41	0.40
Ti	0.27	0.21	0.13	0.25	0.19	0.04	0.16	0.22	0.10	0.03	0.01	0.15	0.16	0.26	0.16	0.17	0.19	0.17	0.20	0.16	0.17
Fe^{3+}	0.54	0.44	0.70	0.46	0.37	0.59	0.36	0.49	0.46	1.05	0.72	0.56	0.55	0.54	0.49	0.65	0.35	0.49	0.30	0.34	0.52
Cr	0.00	0.01	0.01	0.00	0.00	0.00	0.00	0.00	0.00	0.00	0.00	0.00	0.00	0.00	0.00	0.00	0.00	0.00	0.00	0.00	0.00
Mg	1.54	1.38	1.57	1.35	1.62	1.65	1.46	1.34	1.68	1.46	1.34	1.75	1.64	1.41	1.77	1.77	1.71	1.70	1.72	1.46	1.37
Fe^{2+}	2.35	2.58	2.23	2.55	2.44	2.29	2.56	2.58	2.37	2.01	2.32	2.31	2.31	2.47	2.32	2.21	2.47	2.34	2.43	2.57	2.47
Mn^{3+}	0.06	0.04	0.00	0.07	0.03	0.04	0.06	0.06	0.07	0.01	0.01	0.07	0.04	0.09	0.08	0.05	0.05	0.07	0.05	0.06	0.07
Sum C	5.00	5.00	5.00	5.00	5.00	5.00	5.00	5.00	5.00	5.00	5.00	5.00	5.00	5.00	5.00	5.00	5.00	5.00	5.00	5.00	5.00
Mg	0.00	0.00	0.00	0.00	0.00	0.00	0.00	0.00	0.00	0.00	0.00	0.00	0.00	0.00	0.00	0.00	0.00	0.00	0.00	0.00	0.00
Fe^{2+}	0.00	0.00	0.01	0.00	0.00	0.00	0.00	0.00	0.00	0.00	0.00	0.00	0.00	0.00	0.00	0.00	0.00	0.00	0.00	0.00	0.00
Mn^{2+}	0.04	0.03	0.08	0.04	0.05	0.03	0.04	0.04	0.03	0.08	0.06	0.03	0.05	0.02	0.02	0.04	0.03	0.03	0.03	0.03	0.03
Ca	1.91	1.93	1.81	1.92	1.89	1.94	1.92	1.91	1.94	1.83	1.86	1.94	1.90	1.96	1.95	1.92	1.94	1.93	1.93	1.95	1.94
Na	0.05	0.04	0.10	0.04	0.06	0.03	0.04	0.05	0.03	0.09	0.07	0.03	0.05	0.02	0.03	0.04	0.03	0.04	0.04	0.03	0.03
Sum B	2.00	2.00	2.00	2.00	2.00	2.00	2.00	2.00	2.00	2.00	2.00	2.00	2.00	2.00	2.00	2.00	2.00	2.00	2.00	2.00	2.00
Na	0.32	0.31	0.19	0.31	0.25	0.28	0.24	0.28	0.27	0.34	0.30	0.29	0.24	0.35	0.33	0.28	0.29	0.24	0.30	0.29	0.26
K	0.29	0.33	0.37	0.31	0.25	0.21	0.30	0.32	0.21	0.21	0.22	0.24	0.29	0.32	0.25	0.24	0.23	0.24	0.27	0.31	0.28
Sum A	0.61	0.64	0.56	0.61	0.50	0.50	0.54	0.59	0.49	0.55	0.53	0.52	0.53	0.67	0.58	0.51	0.52	0.48	0.57	0.60	0.54
Total	15.61	15.64	15.56	15.61	15.50	15.50	15.54	15.59	15.49	15.55	15.53	15.52	15.53	15.67	15.58	15.51	15.52	15.48	15.57	15.60	15.54
$(Mg+Fe^{2+}+Mn^{2+})$	3.99	4.04	3.89	4.01	4.15	4.01	4.13	4.02	4.14	3.56	3.73	4.16	4.05	3.98	4.19	4.07	4.27	4.14	4.23	4.11	3.93
$Mg/Mg+Fe^{2+}$	0.40	0.35	0.41	0.35	0.40	0.42	0.36	0.34	0.42	0.42	0.37	0.43	0.42	0.36	0.43	0.44	0.41	0.42	0.41	0.36	0.36
$(Ca+Na)_B$	1.96	1.97	1.91	1.96	1.95	1.97	1.96	1.96	1.97	1.92	1.94	1.97	1.95	1.98	1.98	1.96	1.97	1.97	1.97	1.97	1.97
$(Na+K)_A$	0.61	0.64	0.56	0.61	0.50	0.50	0.54	0.59	0.49	0.55	0.53	0.52	0.53	0.67	0.58	0.51	0.52	0.48	0.57	0.60	0.54

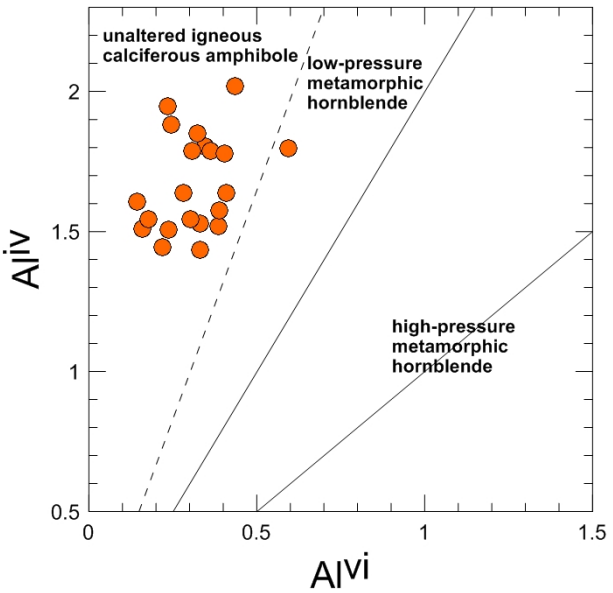

Figure 9. Al^{IV} vs. Al^{VI} calcic amphibole discrimination diagram showing the fields of igneous and metamorphic amphiboles (after Fleet and Barnett, 1978).

discussed in the thermobarometry section, the mafic end member of our study area has a temperature of about 1160 ºC and the granitic melt has a crystallization temperature of about 803 ºC. This difference in temperature results in pronounced viscosity and density contrasts restricting the mixing of magmas at first. Diffusion of heat will slowly lead to attainment of thermal equilibrium. For the hybrid rocks of our study, we have attained average crystallization temperature of 804 ºC, that is lower than the initial basaltic magma temperature but correspond to the temperature of granitic magma, suggesting thermal equilibration. A recent work by Xiong et al. (2012) has shown that mafic magmatic enclaves (MME) and their host granodiorites have crystallized under the same P-T conditions.

Chemical equilibration

Once thermal equilibrium is attained between the two compositionally distinct magmas, the rheological contrasts between the two entities decreased, allowing chemical diffusion to take place (Frost and Mahood, 1987; Foster and Hyndman, 1990; Christiansen and Venchiarutti, 1990). It has been experimentally predicted that volatiles, K, P, Ba, Rb, Sr, Zr, Nb and light REE all have a tendency to rapidly migrate from the felsic to the mafic phase during magma interaction (Watson and Jurewicz, 1984; Johnston and Wyllie, 1988; Baker, 1990; Tate et al., 1997). The migration of these large numbers of elements definitely has a control on the crystallization behaviour of the mafic magma. However, in our case it cannot be ruled out that mafic melt crystallised minerals before thermo-chemical equilibration ensued. We envisage that it is the hydration crystallisation of anhydrous mafic minerals such as clinopyroxene, calcic plagioclase and Fe -Ti oxides in the presence of hydrous granitic melt has resulted in the formation of amphibole and biotite as observed in the hybrids. Such reactions are common place in felsic-mafic interactions and happen at relatively low temperatures (<1000 ºC) (Beard et al., 2003; Beard et al., 2004; Beard et al., 2005: opx+cpx+oxides+calcic plag+hydrous melt = amphibole and/or mica+quartz+sodic plagioclase).

Even if we consider the crystallisation process to have begun after thermal equilibrium, petrography and mineral chemical observations show that amphibole and plagioclase were the dominant minerals to have crystallised from the mafic melt initially after thermal equilibrium with minor proportion of biotite. Further reaction between the amphibole bearing mafic rocks and hydrous K-rich felsic melts or fluids would have resulted in further addition of biotite to the system via reaction:

$Ca_2Mg_5Si_8O_{22}(OH)_2+0.5K_2O(m)+0.5Al_2O_3(m)=$
$KMg_3AlSi_3O_{10}(OH)_2+2CaO(m)+ MgO(m)+5SiO_2(m)$
(Farner et al., 2014)

Disequilibrium textures like altered and resorbed grains of amphibole and biotite and compositional zonings in plagioclase (See Figure 3 d,f) supports our argument.

Back-veining

The decrease in viscosity due to heating of the colder felsic magma by the hotter mafic magma causes reduction in viscosity contrast between the two entities, which allows felsic magma to back-vein the mafic magma (Blake, 1981; Vernon et al., 1988). Petrographic observations have revealed that the hybrid rock contains large anhedral grains/masses of K-feldspar and quartz that have embedded grains of earlier crystallized minerals (i.e., amphibole, plagioclase and biotite; Figure 3e) which are part of the mafic component. The influx of felsic melt into the mafic system resulted in this embedded texture. Moreover, the influx of felsic melt into the mafic system led to the destabilization of amphibole and biotite to form liquids of titanite composition. These newly formed titanite liquids were assimilated by the incoming felsic melt and flowed along with it as a separate immiscible phase through the crystal dominated mafic matrix. Vegas et al. (2011) suggested that the genesis of titanite-centered ocellar texture is due to the interaction of late-stage residual melt with Ti-rich biotite which increases the T-concentration in the former. This Ti-rich melt, in turn, was responsible for the formation of titanite ocelli in the

Table 6. Representative electron microprobe analyses of biotite in wt% oxide from the mafic end-member.

SiO_2	40.97	38.46	37.07	38.76	38.08	37.91	38.42	35.83	36.90	36.20	36.41
TiO_2	0.16	1.46	1.50	1.18	1.81	1.84	1.36	1.58	1.64	1.39	1.28
Al_2O_3	11.20	13.23	13.61	13.19	13.80	13.92	14.50	14.67	15.95	14.89	16.14
FeO	20.78	20.55	21.15	19.57	19.70	20.35	19.07	22.44	19.95	21.94	20.19
MnO	0.15	0.16	0.07	0.06	0.14	0.09	0.15	0.31	0.31	0.18	0.13
MgO	12.96	11.16	10.38	11.01	10.50	10.40	11.07	9.25	9.72	9.67	9.40
CaO	0.00	0.06	0.01	0.04	0.06	0.05	1.04	0.00	0.25	0.00	0.05
Na_2O	0.03	0.09	0.08	0.04	0.02	0.04	0.08	0.01	0.03	0.07	0.06
K_2O	7.08	7.89	7.94	7.72	7.82	7.80	8.49	8.05	8.69	7.55	8.22
Cl	0.10	0.48	0.59	0.41	0.17	0.08	0.04	0.52	0.07	0.82	0.07
F	0.07	0.02	0.29	0.00	0.06	0.00	0.43	0.19	0.20	0.12	0.13
BaO	0.00	0.00	0.00	0.00	0.34	0.00	0.14	0.00	0.27	0.00	0.39
Totals	93.50	93.54	92.70	91.97	92.51	92.47	94.77	92.84	93.98	92.83	92.49
Calculation based on eleven oxygens											
Si	3.14	2.97	2.90	3.02	2.97	2.96	2.91	2.83	2.85	2.84	2.85
Al^{IV}	0.86	1.03	1.10	0.98	1.03	1.04	1.09	1.17	1.15	1.16	1.15
Sum T	4.00	4.00	4.00	4.00	4.00	4.00	4.00	4.00	4.00	4.00	4.00
Al^{vi}	0.14	0.17	0.15	0.23	0.23	0.24	0.21	0.19	0.30	0.21	0.34
Ti	0.01	0.08	0.09	0.07	0.11	0.11	0.08	0.09	0.10	0.08	0.08
Fe	1.33	1.33	1.38	1.28	1.28	1.33	1.21	1.48	1.29	1.44	1.32
Mn	0.01	0.01	0.00	0.00	0.01	0.01	0.01	0.02	0.02	0.01	0.01
Mg	1.48	1.28	1.21	1.28	1.22	1.21	1.25	1.09	1.12	1.13	1.10
Sum Y	2.97	2.88	2.83	2.86	2.85	2.89	2.75	2.87	2.82	2.87	2.85
Ca	0.00	0.00	0.00	0.00	0.00	0.00	0.08	0.00	0.02	0.00	0.00
Na	0.00	0.01	0.01	0.01	0.00	0.01	0.01	0.00	0.01	0.01	0.01
K	0.69	0.78	0.79	0.77	0.78	0.78	0.82	0.81	0.86	0.75	0.82
Ba	0.00	0.00	0.00	0.00	0.01	0.00	0.00	0.00	0.01	0.00	0.01
Sum X	0.69	0.79	0.80	0.78	0.80	0.79	0.92	0.81	0.89	0.77	0.85
F	0.02	0.01	0.07	0.00	0.02	0.00	0.10	0.05	0.05	0.03	0.03
Cl	0.01	0.06	0.08	0.05	0.02	0.01	0.01	0.07	0.01	0.11	0.01
$Fe+Mn+Ti-Al^{VI}$	1.20	1.25	1.33	1.12	1.17	1.20	1.09	1.40	1.11	1.32	1.06
Fe+Mg	2.81	2.61	2.59	2.55	2.50	2.54	2.46	2.57	2.40	2.57	2.42
Fe/Fe+Mg	0.47	0.51	0.53	0.50	0.51	0.52	0.49	0.58	0.54	0.56	0.55

hybrid rocks of their study area.

The association of titanite-liquid and felsic melt could not be traced in the hybrid rocks of NGP due to advanced stage of magma mixing. This unique association has been observed in the hybrid rocks of Ghansura Rhyolite Dome (GRD). The GRD is a part of the BVSs located at a distance of about 3 km from the NGP. Magma mixing signatures are also preserved in the rhyolite domain. In the hybrid rocks of GRD, liquids of titanite composition have been observed migrating from mafic phase to felsic phase; now preserved as mineral veins in the hybrid rocks (Figure 12a). The existence of such veins suggests that liquids of titanite composition can form in a magma mixing scenario in the mafic phase, possibly due to destabilization of mafic minerals like amphibole and biotite. Furthermore, the migration of titanite (liquid) from the mafic phase to the felsic phase suggests that such liquids have greater affinity to be incorporated by the felsic

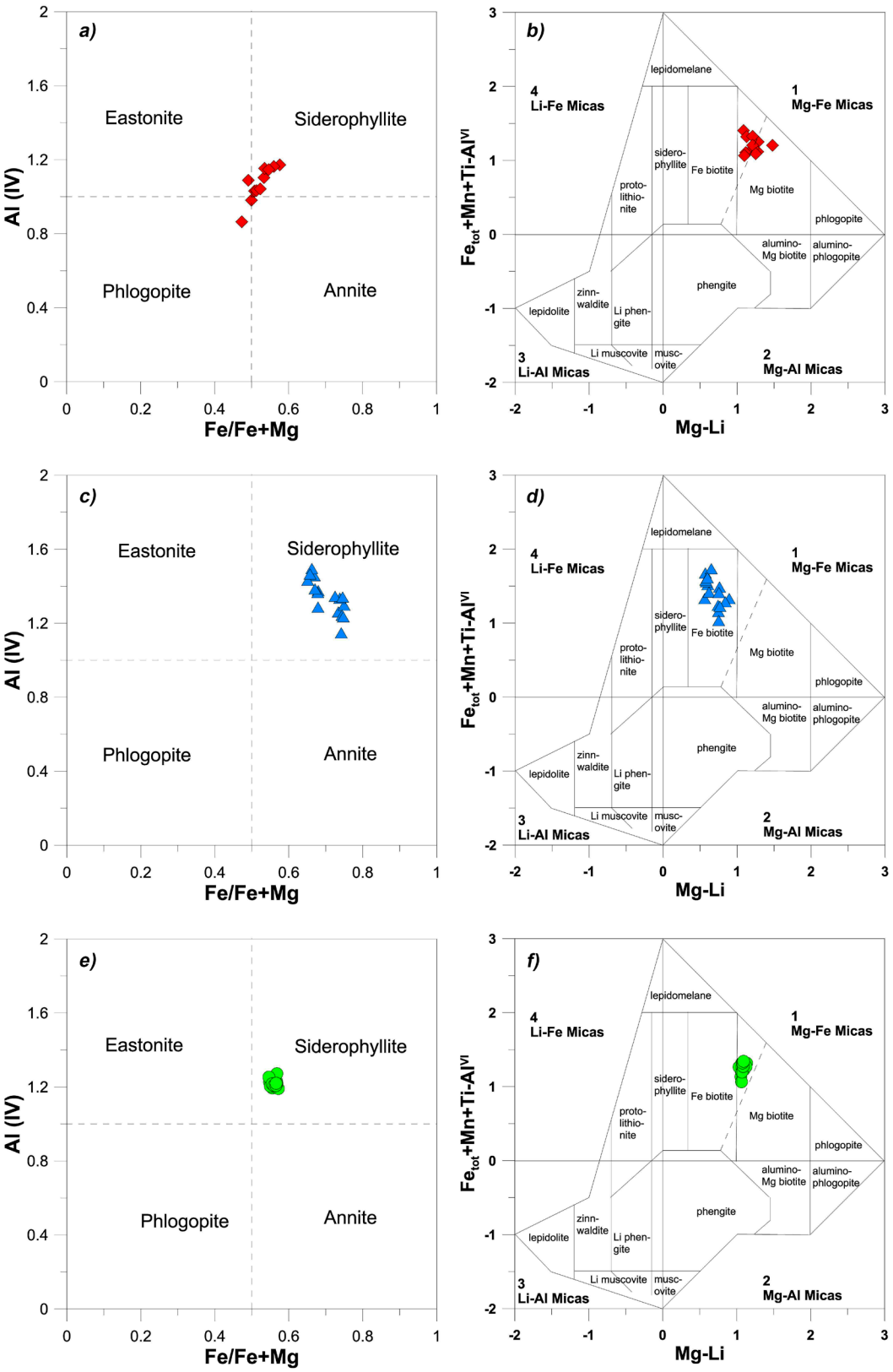

Figure 10. Nomenclature and classification of biotites occurring in the a, b) mafic end-member; c, d) felsic end-member; e, f) matrix of the hybrid rock displaying titanite ocelli (Deer et al., 1980; Rieder et al., 1998; Tischendorf, 1997).

Table 7. Representative electron microprobe analyses of biotite in wt% oxide from the felsic end-member.

SiO_2	33.29	34.66	33.83	34.22	32.57	32.90	32.64	33.79	35.36	34.61	34.82	35.20	33.86	36.31	34.41	34.12
TiO_2	1.26	1.95	1.20	1.71	1.09	0.70	0.89	0.87	1.90	2.66	2.14	1.79	1.77	1.32	1.59	1.52
Al_2O_3	21.12	16.74	19.61	18.23	22.12	19.78	20.27	19.57	17.12	16.65	16.73	16.51	17.09	16.79	18.87	17.73
FeO	23.72	24.66	24.32	24.70	22.90	25.56	24.81	24.16	25.67	26.10	25.59	26.00	27.93	24.57	25.42	26.96
MnO	0.20	0.24	0.15	0.16	0.12	0.14	0.18	0.14	0.75	0.77	0.79	0.87	0.62	0.67	0.85	0.82
MgO	6.58	6.54	6.43	6.57	6.55	7.68	7.26	6.65	5.22	4.89	4.94	4.93	5.56	4.79	5.40	5.15
CaO	0.01	0.00	0.00	0.00	0.06	0.00	0.10	0.00	0.00	0.00	0.00	0.00	0.04	0.42	0.00	0.00
Na_2O	0.10	0.02	0.09	0.05	0.10	0.05	0.03	0.11	0.06	0.13	0.05	0.07	0.03	0.00	0.11	0.04
K_2O	8.99	9.41	8.96	9.24	9.11	7.31	8.01	9.05	8.70	8.93	9.22	8.87	7.87	8.46	8.52	9.01
Cl	0.05	0.04	0.01	0.04	0.07	0.04	0.04	0.06	0.02	0.02	0.02	0.03	0.03	0.02	0.05	0.02
F	0.74	0.62	0.57	0.94	0.58	0.40	0.67	0.76	0.78	0.77	0.35	0.67	0.55	0.51	0.72	0.78
BaO	0.13	0.01	0.00	0.25	0.21	0.00	0.08	0.01	0.38	0.24	0.00	0.00	0.40	0.00	0.09	0.07
Totals	96.20	94.88	95.16	96.10	95.48	94.57	94.98	95.17	95.97	95.78	94.64	94.92	95.73	93.87	96.04	96.22
Calculation based on eleven oxygens																
Si	2.54	2.71	2.62	2.63	2.51	2.57	2.53	2.61	2.74	2.70	2.76	2.77	2.66	2.85	2.65	2.66
Al^{IV}	1.46	1.29	1.38	1.37	1.50	1.43	1.47	1.39	1.26	1.30	1.24	1.23	1.34	1.15	1.35	1.34
Sum T	4.00	4.00	4.00	4.00	4.00	4.00	4.00	4.00	4.00	4.00	4.00	4.00	4.00	4.00	4.00	4.00
Al^{vi}	0.44	0.26	0.42	0.29	0.51	0.39	0.39	0.40	0.30	0.24	0.32	0.29	0.25	0.41	0.37	0.29
Ti	0.07	0.11	0.07	0.10	0.06	0.04	0.05	0.05	0.11	0.16	0.13	0.11	0.10	0.08	0.09	0.09
Fe	1.52	1.61	1.58	1.59	1.47	1.67	1.61	1.56	1.66	1.70	1.69	1.71	1.84	1.61	1.64	1.76
Mn	0.01	0.02	0.01	0.01	0.01	0.01	0.01	0.01	0.05	0.05	0.05	0.06	0.04	0.04	0.06	0.05
Mg	0.75	0.76	0.74	0.75	0.75	0.89	0.84	0.77	0.60	0.57	0.58	0.58	0.65	0.56	0.62	0.60
Sum Y	2.79	2.77	2.82	2.74	2.81	3.00	2.91	2.79	2.73	2.72	2.77	2.74	2.88	2.70	2.78	2.79
Ca	0.00	0.00	0.00	0.00	0.01	0.00	0.01	0.00	0.00	0.00	0.00	0.00	0.00	0.04	0.00	0.00
Na	0.01	0.00	0.01	0.01	0.01	0.01	0.00	0.02	0.01	0.02	0.01	0.01	0.00	0.00	0.02	0.01
K	0.88	0.94	0.89	0.91	0.89	0.73	0.79	0.89	0.86	0.89	0.93	0.89	0.79	0.85	0.84	0.90
Ba	0.00	0.00	0.00	0.01	0.01	0.00	0.00	0.00	0.01	0.01	0.00	0.00	0.01	0.00	0.00	0.00
Sum X	0.89	0.94	0.90	0.92	0.92	0.74	0.81	0.91	0.88	0.92	0.94	0.90	0.81	0.88	0.86	0.90
F	0.18	0.15	0.14	0.23	0.14	0.10	0.17	0.19	0.19	0.19	0.09	0.17	0.14	0.13	0.18	0.19
Cl	0.01	0.01	0.00	0.01	0.01	0.01	0.01	0.01	0.00	0.00	0.00	0.00	0.00	0.00	0.01	0.00
$Fe+Mn+Ti-Al^{VI}$	1.16	1.49	1.24	1.41	1.03	1.33	1.29	1.23	1.52	1.68	1.56	1.58	1.73	1.33	1.42	1.61
Fe+Mg	2.26	2.38	2.32	2.34	2.22	2.56	2.45	2.33	2.27	2.27	2.28	2.29	2.49	2.18	2.26	2.36
Fe/Fe+Mg	0.67	0.68	0.68	0.68	0.66	0.65	0.66	0.67	0.73	0.75	0.74	0.75	0.74	0.74	0.73	0.75

Table 8. Representative electron microprobe analyses of biotite in wt% oxide from the hybrid rock displaying titanite-centered ocellar texture.

SiO_2	36.01	36.48	36.35	36.20	36.46	36.82	36.39	36.42	36.28	36.71	36.81	36.16	36.92	36.69	36.61	35.94
TiO_2	1.20	1.60	1.37	1.35	1.20	1.20	1.11	1.27	1.67	1.34	1.04	1.33	1.39	1.24	1.34	1.26
Al_2O_3	15.95	16.09	16.66	15.46	15.88	15.72	15.93	15.62	16.84	15.75	17.08	16.24	16.41	15.86	15.53	15.47
FeO	21.25	21.73	20.75	21.46	21.38	21.98	21.96	21.96	21.57	21.32	20.47	21.36	21.18	21.75	21.99	22.02
MnO	0.40	0.39	0.41	0.52	0.43	0.42	0.50	0.47	0.53	0.53	0.46	0.60	0.42	0.49	0.47	0.54
MgO	9.14	9.66	9.21	9.92	9.58	9.24	9.39	9.38	9.20	9.42	9.40	9.95	9.52	9.59	9.48	9.48
CaO	0.04	0.06	0.02	0.07	0.00	0.20	0.00	0.03	0.00	0.05	0.15	0.05	0.14	0.07	0.06	0.04
Na_2O	0.03	0.09	0.09	0.06	0.10	0.08	0.05	0.05	0.07	0.14	0.38	0.11	0.13	0.09	0.09	0.11
K_2O	8.95	8.91	8.98	9.28	9.18	8.91	9.17	9.08	9.32	9.09	8.74	8.98	8.70	8.93	9.01	9.01
Cl	0.03	0.05	0.03	0.02	0.05	0.10	0.09	0.07	0.07	0.09	0.05	0.05	0.06	0.06	0.05	0.04
F	0.73	0.61	0.44	0.80	0.50	0.72	0.93	0.93	0.93	0.84	0.54	0.80	0.85	0.76	0.82	0.66
BaO	0.35	0.29	0.07	0.09	0.03	0.03	0.19	0.13	0.26	0.00	0.08	0.16	0.23	0.00	0.08	0.01
Totals	94.09	95.95	94.38	95.23	94.79	95.40	95.71	95.40	96.73	95.29	95.21	95.79	95.93	95.51	95.52	94.58
Calculation based on eleven oxygens																
Si	2.79	2.77	2.80	2.77	2.81	2.81	2.77	2.78	2.73	2.80	2.80	2.75	2.78	2.79	2.79	2.78
Al^{iv}	1.21	1.23	1.20	1.23	1.19	1.19	1.23	1.22	1.27	1.20	1.20	1.25	1.22	1.21	1.21	1.22
Sum T	4.00	4.00	4.00	4.00	4.00	4.00	4.00	4.00	4.00	4.00	4.00	4.00	4.00	4.00	4.00	4.00
Al^{VI}	0.24	0.22	0.31	0.17	0.24	0.22	0.20	0.19	0.22	0.21	0.32	0.20	0.24	0.21	0.19	0.19
Ti	0.07	0.09	0.08	0.08	0.07	0.07	0.06	0.07	0.09	0.08	0.06	0.08	0.08	0.07	0.08	0.07
Fe	1.38	1.38	1.34	1.37	1.38	1.40	1.40	1.40	1.36	1.36	1.30	1.36	1.34	1.38	1.40	1.42
Mn	0.03	0.02	0.03	0.03	0.03	0.03	0.03	0.03	0.03	0.03	0.03	0.04	0.03	0.03	0.03	0.04
Mg	1.05	1.09	1.06	1.13	1.10	1.05	1.07	1.07	1.03	1.07	1.06	1.13	1.07	1.09	1.08	1.09
Sum Y	2.77	2.81	2.81	2.79	2.82	2.77	2.76	2.76	2.74	2.75	2.78	2.80	2.75	2.79	2.78	2.82
Ca	0.00	0.01	0.00	0.01	0.00	0.02	0.00	0.00	0.00	0.00	0.01	0.00	0.01	0.01	0.00	0.00
Na	0.00	0.01	0.01	0.01	0.01	0.01	0.01	0.01	0.01	0.02	0.06	0.02	0.02	0.01	0.01	0.02
K	0.88	0.86	0.88	0.91	0.90	0.87	0.89	0.88	0.89	0.88	0.85	0.87	0.84	0.87	0.88	0.89
Ba	0.01	0.01	0.00	0.00	0.00	0.00	0.01	0.00	0.01	0.00	0.00	0.00	0.01	0.00	0.00	0.00
Sum X	0.90	0.89	0.90	0.92	0.92	0.90	0.90	0.90	0.91	0.91	0.92	0.90	0.87	0.89	0.90	0.91
F	0.18	0.15	0.11	0.19	0.12	0.17	0.22	0.22	0.22	0.20	0.13	0.19	0.20	0.18	0.20	0.16
Cl	0.00	0.01	0.00	0.00	0.01	0.01	0.01	0.01	0.01	0.01	0.01	0.01	0.01	0.01	0.01	0.01
$Fe+Mn+Ti-Al^{VI}$	1.23	1.28	1.13	1.32	1.23	1.28	1.29	1.32	1.26	1.26	1.07	1.27	1.20	1.27	1.32	1.34
Fe+Mg	2.43	2.48	2.39	2.51	2.47	2.45	2.46	2.47	2.39	2.43	2.36	2.48	2.41	2.47	2.48	2.52
Fe/Fe+Mg	0.57	0.56	0.56	0.55	0.56	0.57	0.57	0.57	0.57	0.56	0.55	0.55	0.56	0.56	0.57	0.57

Table 9. Representative electron microprobe analyses of titanite in wt% oxide from the hybrid rock displaying titanite-centered ocellar texture.

	Inclusion in amphibole					Matrix						In ocelli							
SiO_2	30.66	30.27	30.47	30.50	30.60	30.32	30.60	30.65	30.55	30.74	30.87	29.56	29.26	29.36	29.95	30.38	30.00	29.12	29.29
TiO_2	33.98	33.75	34.54	34.43	35.47	34.61	33.43	33.24	33.46	35.33	33.95	34.51	32.67	34.21	32.91	35.28	33.29	33.63	34.03
Al_2O_3	2.61	2.86	2.10	2.51	3.95	2.66	2.66	2.53	2.97	2.70	3.63	1.61	1.84	1.81	1.99	1.91	1.98	1.60	1.79
FeO	1.43	1.24	1.15	1.16	1.11	1.19	1.21	1.32	1.18	0.91	1.30	1.05	1.32	1.23	1.21	1.28	1.39	0.98	1.23
MnO	0.04	0.08	0.18	0.12	0.00	0.08	0.21	0.07	0.13	0.12	0.07	0.04	0.10	0.00	0.09	0.00	0.17	0.14	0.13
MgO	0.02	0.02	0.00	0.00	0.06	0.00	0.00	0.01	0.01	0.00	0.02	0.03	0.02	0.00	0.02	0.03	0.04	0.00	0.00
CaO	28.82	28.42	28.65	28.47	28.69	28.93	28.55	28.58	28.76	29.16	29.35	27.03	27.12	27.16	27.45	28.00	28.09	27.24	27.61
Na_2O	0.00	0.00	0.02	0.00	0.00	0.00	0.00	0.01	0.01	0.00	0.00	0.04	0.02	0.02	0.03	0.04	0.05	0.03	0.02
K_2O	0.01	0.02	0.01	0.00	0.13	0.00	0.01	0.02	0.01	0.03	0.07	0.00	0.00	0.00	0.00	0.00	0.00	0.00	0.00
Cl	0.01	0.01	0.00	0.00	0.00	0.00	0.00	0.00	0.00	0.00	0.01	0.01	0.02	0.00	0.01	0.00	0.00	0.00	0.02
F	0.93	0.83	0.73	0.80	1.16	0.29	0.45	0.86	0.53	0.73	1.37	0.26	0.00	0.19	0.27	0.16	0.54	0.29	0.65
BaO	0.21	0.00	0.00	0.21	0.08	0.02	0.06	0.00	0.02	0.25	0.11	0.08	0.39	0.12	0.00	0.19	0.14	0.17	0.00
Total	98.71	97.48	97.84	98.20	101.24	98.11	97.16	97.29	97.63	99.96	100.74	94.22	92.75	94.09	93.92	97.27	95.69	93.19	94.76
Calculation based on twenty oxygens																			
Si	4.03	4.02	4.04	4.03	3.90	4.03	4.10	4.08	4.06	3.99	3.95	4.08	4.14	4.07	4.15	4.08	4.09	4.08	4.02
Ti	3.36	3.37	3.45	3.42	3.40	3.46	3.37	3.33	3.35	3.45	3.27	3.59	3.48	3.57	3.43	3.56	3.41	3.54	3.51
Al	0.40	0.45	0.33	0.39	0.59	0.42	0.42	0.40	0.47	0.41	0.55	0.26	0.31	0.30	0.32	0.30	0.32	0.26	0.29
Fe	0.16	0.14	0.13	0.13	0.12	0.13	0.14	0.15	0.13	0.10	0.14	0.12	0.16	0.14	0.14	0.14	0.16	0.11	0.14
Mn	0.00	0.01	0.02	0.01	0.00	0.01	0.02	0.01	0.02	0.01	0.01	0.01	0.01	0.00	0.01	0.00	0.02	0.02	0.01
Mg	0.00	0.00	0.00	0.00	0.01	0.00	0.00	0.00	0.00	0.00	0.00	0.01	0.00	0.00	0.00	0.01	0.01	0.00	0.00
Ca	4.06	4.04	4.07	4.03	3.91	4.12	4.09	4.07	4.10	4.06	4.02	4.00	4.11	4.04	4.07	4.03	4.10	4.09	4.06
Na	0.00	0.00	0.00	0.00	0.00	0.00	0.00	0.00	0.00	0.00	0.00	0.01	0.00	0.01	0.01	0.01	0.01	0.01	0.00
K	0.00	0.00	0.00	0.00	0.02	0.00	0.00	0.00	0.00	0.00	0.01	0.00	0.00	0.00	0.00	0.00	0.00	0.00	0.00
Cl	0.00	0.00	0.00	0.00	0.00	0.00	0.00	0.00	0.00	0.00	0.00	0.00	0.01	0.00	0.00	0.00	0.00	0.00	0.00
F	0.38	0.35	0.30	0.33	0.47	0.12	0.19	0.36	0.22	0.30	0.55	0.11	0.00	0.08	0.12	0.07	0.23	0.13	0.28
Ba	0.01	0.00	0.00	0.01	0.00	0.00	0.00	0.00	0.00	0.01	0.01	0.00	0.02	0.01	0.00	0.01	0.01	0.01	0.00
Total	12.41	12.39	12.35	12.35	12.42	12.30	12.33	12.40	12.35	12.35	12.51	12.20	12.23	12.21	12.26	12.21	12.35	12.25	12.32

Table 10. Representative major, trace and rare earth element compositions of the mafic, felsic and hybrid rocks from NGP.

Rock type	Mafic					Felsic					Hybrid				
Sample	RD2C	RD30FM	RD30C	RD30DM	RD4	RD28	RD14	RD35	RD29F	RD25	RD7	RD10	RD12	RD13	RD16E
SiO_2	47	49.54	47.11	47.77	47.44	69.80	68.50	70.47	70.57	69.87	52.46	52.63	53.57	59.4	54.03
TiO_2	1.89	2.99	1.43	1.5	2.06	0.26	0.24	0.21	0.21	0.25	1.10	0.92	0.98	0.9	1.01
Al_2O_3	14.84	13.04	15.33	14.81	14.61	15.22	15.33	15.45	15.03	15.81	15.66	11.91	13.8	15.81	13.58
Fe_2O_3	13.82	16.34	12.25	12.52	14.16	2.99	3.20	2.57	2.62	2.23	10.77	10.17	9.9	7.93	10.63
MnO	0.18	0.21	0.17	0.18	0.20	0.07	0.08	0.06	0.06	0.02	0.20	0.16	0.14	0.12	0.22
MgO	7.2	3.54	8.09	8.2	7.28	0.61	0.57	0.50	0.52	0.55	4.55	7.96	6.07	3.05	6.66
CaO	8.47	8.35	9.39	9.71	9.06	1.69	1.89	1.61	1.57	2.04	6.31	10.03	8.35	4.3	7.64
Na_2O	2.35	4.13	2.1	2.1	2.37	3.33	3.46	3.38	3.20	3.13	2.88	1.82	2.16	3.16	2.93
K_2O	1.19	0.28	0.81	0.7	0.68	4.63	4.62	4.83	4.68	4.30	3.06	2.02	2.45	4.18	1.81
P_2O_5	0.25	0.44	0.19	0.15	0.22	0.15	0.14	0.13	0.13	0.11	0.43	0.28	0.37	0.39	0.34
LOI	2.04	1.60	2.14	2.12	1.40	0.81	1.58	0.80	0.85	0.78	0.96	1.48	1.54	1.06	1.17
Total	99.23	100.46	99.01	99.76	99.48	99.56	99.61	100.01	99.44	99.09	98.38	99.38	99.33	100.3	100.02
Ba	0	0	12	32	0	461	517	442	456	984	522	321	345	715	352
Co	1032	0	1573	1029	3067	2	3	7	4	7	24	43	31	12	29
Cr	132	92	204	222	165	201	221	220	178	184	124	220	331	146	355
Cu	36	42	46	49	36	4	3	6	4	9	27	62	62	13	16
Ga	18	20	15	17	15	22	22	19	18	18	23	16	18	20	21
Nb	13	24	9	10	12	21	16	17	23	14	16	9	12	22	18
Ni	79	4	102	99	75	4	3	1	0	2	5	58	31	9	66
Pb	3	4	2	6	7	35	40	43	43	35	16	13	13	23	14
Rb	73	12	58	56	56	346	292	292	322	145	247	77	134	215	159
Sc	25	33	32	39	22	8	2	13	0	18	20	43	36	15	31
Sr	280	148	259	222	215	177	165	157	157	219	340	276	324	324	298
Th	3	4	4	2	0	37	37	34	31	23	14	11	14	19	25
U	1	1	1	1	2	10	6	8	11	0	5	2	3	3	6
V	270	344	236	254	328	13	12	12	12	20	193	240	179	82	189
Y	31	45	26	28	30	46	40	40	41	12	44	31	38	35	40
Zn	106	65	95	94	111	48	57	61	45	30	127	91	82	84	114
Zr	120	208	97	98	117	177	145	141	150	178	147	109	128	215	185
La	12.5	26.6	9.3	10.3	13.4	36.4	35.8	37.1	34.9	85.1	42	30.4	23.6	58	44
Ce	29.6	63.2	22.2	24.5	31.8	84.2	83	85.6	81	210.5	89.8	62.5	58.3	117	100
Pr	4.2	8.9	3.2	3.5	4.5	9	9	9.2	8.5	23.9	10.9	7.8	8.1	14	12
Nd	18.3	38.7	14	15.4	19.7	32.9	33.1	34.1	32	94.7	42.6	29.4	32.9	45	50
Sm	4.52	9.24	3.58	3.89	4.79	7.79	7.83	7.84	7.5	21.04	7.38	5.57	7.61	8	10
Eu	1.61	2.98	1.26	1.36	1.59	0.09	0.09	0.08	0.08	0.23	1.81	1.59	1.64	2	2
Gd	4.92	10.17	3.96	4.34	5.32	4.25	4.39	4.05	4.26	10.53	7.17	6.39	8.18	10	9
Tb	0.77	1.66	0.65	0.7	0.84	0.74	0.78	0.71	0.73	1.54	0.95	0.89	1.08	1	1
Dy	4.61	9.69	3.86	4.16	5.05	3.91	4.16	3.45	3.59	5.19	4.86	4.41	5.38	6	5
Ho	0.95	1.99	0.8	0.86	1.05	0.73	0.77	0.6	0.64	0.71	0.99	0.85	1.08	1	1
Er	2.48	5.24	2.1	2.23	2.7	2	2.14	1.54	1.7	1.64	2.75	2.19	2.76	3	3
Tm	0.36	0.78	0.31	0.34	0.4	0.32	0.36	0.25	0.26	0.19	0.41	0.31	0.4	0	0
Yb	2.33	5.1	2.01	2.11	2.51	2.22	2.48	1.56	1.69	0.99	2.9	2.17	2.18	3	3
Lu	0.34	0.75	0.29	0.31	0.36	0.5	0.5	0.37	0.38	0.2	0.45	0.29	0.33	0	0

Major elements are given in wt%, trace and rare earth elememts in ppm. LOI is Loss on ignition.

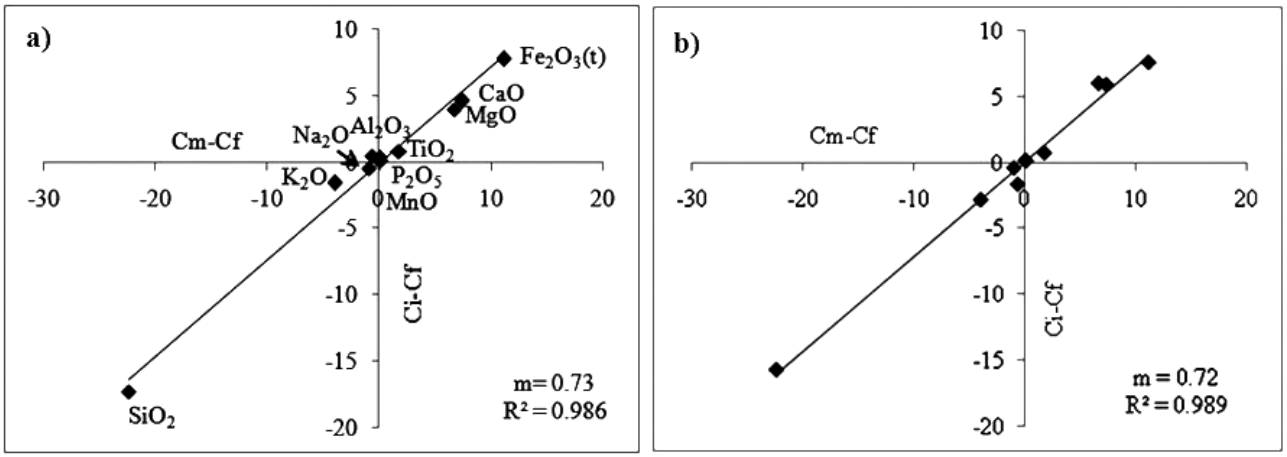

Figure 11. (a, b) Major-oxides mixing test of Fourcade and Allégre (1981) for hybrid rocks displaying titanite ocelli. Cf=concentration of an element in felsic magma, Cm=concentration of an element in mafic magma, Ci=concentration of an element in hybrid magma, m=fraction of mafic magma in the mixture, R^2=correlation coefficient.

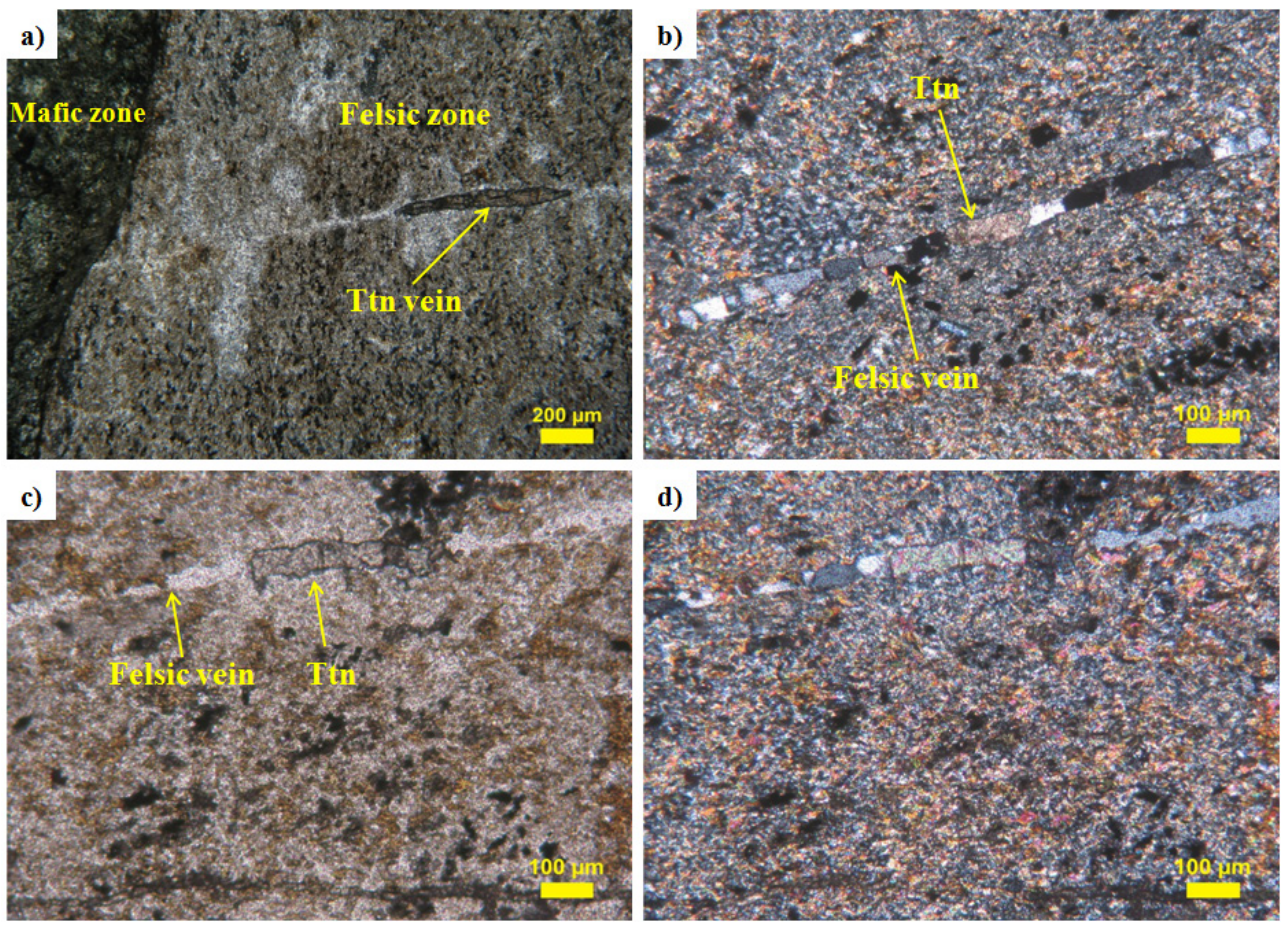

Figure 12. Photomicrographs from the hybrid rocks of Ghansura Rhyolite Dome displaying a) a titanite vein migrating from the mafic zone to the felsic zone. The nature of titanite in the vein suggests that it was flowing as a liquid while traversing through the felsic zone; b-d) a felsic vein containing isolated anhedral patches of titanite. Note that titanite occurring in the vein is covering the entire width of the latter. This textural evidence suggests that titanite formed from a liquid of similar composition which flowed along with the felsic melt as a separate immiscible phase rather than crystallizing from the felsic melt.

melt. Moreover, felsic veins are preserved containing anhedral masses of titanite in the hybrid rocks of GRD (Figure 12 b-d). The occurrence of isolated patches of titanite covering the entire width of the felsic veins clearly indicates that titanite did not crystallized from the felsic melt; rather it flowed along with the felsic melt as a separate immiscible phase. Had titanite crystallized from the felsic melt, small crystals of the mineral would have been distributed throughout the vein rather than occurring as individual patches. The unique association of titanite-liquid and felsic melt has been highlighted on the basis of petrographical evidence observed in the hybrid rocks of GRD.

Occupancy of vesicles

One striking feature of titanite-centered ocellar texture observed in our study is the spherical shape of the ocelli. The observation of the mafic rocks of the BVSs reveals that there is abundance of vesicles in these rocks mostly filled by secondary minerals like calcite and chlorite. The size and shape of the spherical ocelli corresponds to these vesicles. From this we can infer that the escape of volatiles from the mafic magma created low pressure zones in the mafic system, which were occupied by incoming felsic melt and liquid of titanite composition resulting in the formation of titanite-centered ocelli in the vacuum left by escaping of volatiles from the vesicles. The occupancy of vesicles by late-stage residual melt, which leads to the formation of titanite along with other mineral phases in the vesicles, has been described by McLeod et al. (2011). The felsic melt that occupied the void spaces left behind after the escape of volatiles from the vesicles also carried with them crystallized plagioclase grains which were mostly of labradorite composition. In the ocelli, plagioclase started to grow in equilibrium with the new melt in which labradorite plagioclase were overgrown by the andesine plagioclase of the felsic system. Meanwhile, titanite which was present in the melt started crystallizing over some of these crystallizing plagioclase grains. Temperature estimates of our study are suitable for the observed titanite crystallization. Rodriguez et al. (2009) have reported a precise temperature range of 750-780 ºC for crystallization of titanite in their titanite ocelli using Zr in titanite thermometer. A single titanite seems to have taken a single plagioclase grain as a seed to form. In the mean time, plagioclase grains which were not engulfed by titanite continued to grow and equilibrate to an andesine composition. Meanwhile, as the temperature of the system was declining, it resulted in exsolution of albitic plagioclase from the K-feldspars present. This exsolved phase made distinct albitic rims over the previously crystallised plagioclase crystals which were not occurring as inclusions in titanite. The absence of albitic rims in the plagioclase grains present as inclusions in the titanite ocelli suggests that titanite crystallization occurred prior to exsolution of albitic plagioclase from K- feldspar in the felsic melt.

This work attributes the formation of titanite ocelli in a mafic-turned-hybrid system. A number of evidence presented in this paper point toward this inference. Firstly, two of the major mineral phases i.e., plagioclase and biotite occurring in the hybrid rock show compositional similarities with their mafic counterparts (Figures 5, 9). Plagioclase exhibits a rather complex behavior showing compositional zonations and crystals formed by the intruding felsic melt into the mafic domain. Still the cores of most of the plagioclase grains in the hybrid rock are labradorite, which corresponds to the composition of plagioclase occurring in the mafic end-member. Secondly, the major-oxide mixing test (Figure 10) indicates a relative contribution of >70% from the mafic end-member in forming the hybrid product. This large contribution from the mafic magma in forming the titanite ocelli bearing hybrid rock greatly supports the mafic-turned-hybrid process of magma mixing.

CONCLUSIONS

Based on our findings a four-stage model is proposed to account for the sequence of events that led to the formation of titanite ocelli. This is summarized in Figure 13.

Stage 1 involves intrusion of the granitic magma chamber from its bottom by mafic magma. The two disparate magmas remained as separate entities at the time of emplacement of the mafic magma, making no direct interaction with each other. The first interaction that took place between the two contrasting magmas is diffusion of heat from the relatively hotter mafic magma to the colder felsic one. Thus, thermal equilibrium was attained first between the two phases. Once thermal equilibrium was attained, hydration crystallisation of anhydrous mafic minerals such as clinopyroxene, calcic plagioclase and Fe -Ti oxides in the presence of hydrous granitic melt resulted in the formation of amphibole and biotite as observed in the hybrids. After thermochemical equilibration there came a point when the rheological contrasts between the mafic and felsic magmas greatly reduced. This allowed the felsic melt to intrude into the mafic phase. The intrusion of felsic melt disturbed the equilibrium conditions under which minerals were crystallizing in the mafic system. This led to the alteration and destabilization of already crystallized amphibole and biotite. Meanwhile, plagioclase continued to grow with different composition over the initially formed grains. The destabilization of amphibole and biotite released liquids of titanite composition. These liquids were incorporated into the incoming felsic phase and began to flow with it

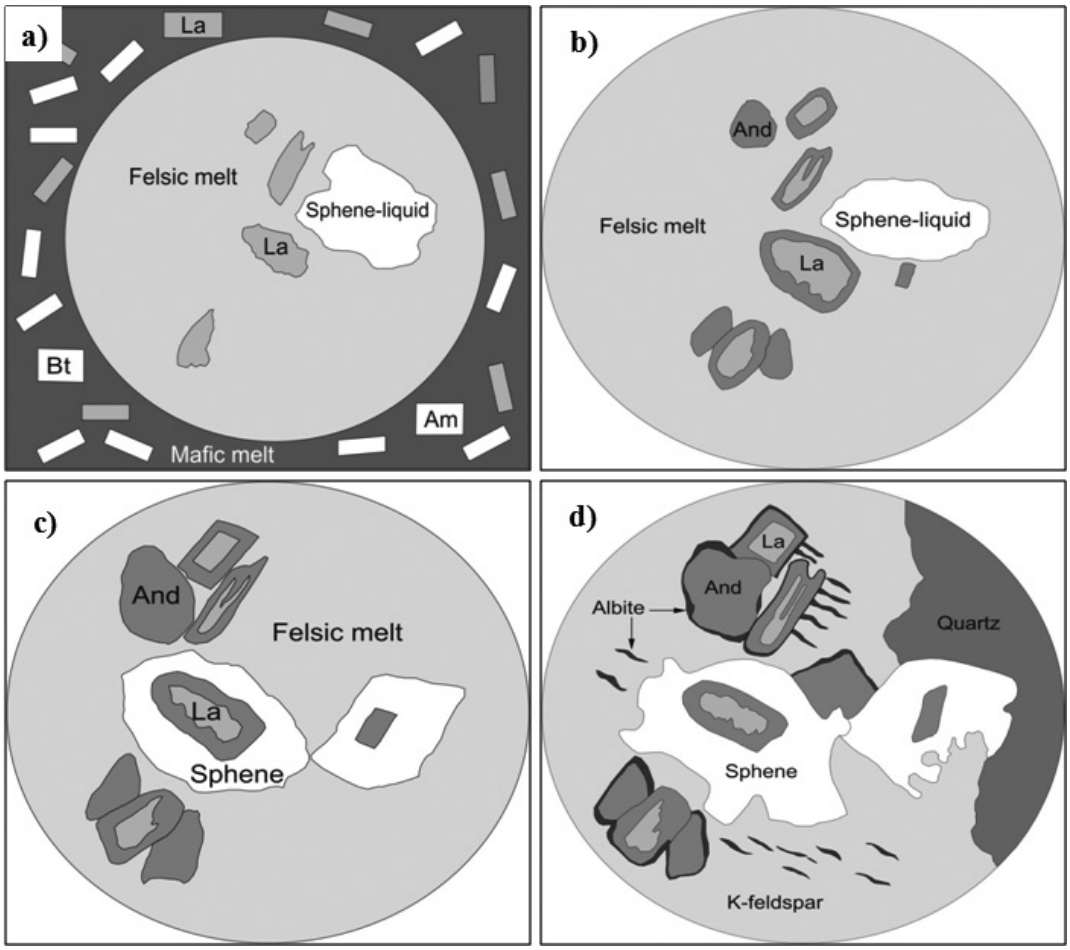

Figure 13. A four-stage model proposed for the formation of titanite ocelli a) Mixture of felsic melt, titanite liquid and labradorite crystals occupy the void spaces left behind by escaping gases/volatiles in the disequilibrated mafic system. b) The labradorite crystals are overgrown by andesine and also new andesine crystals start to crystallize. c) A few crystallizing plagioclase grains become seeds for titanite crystallization which inhibits their further growth. d) With decrease in temperature, K-feldspar and quartz begin to crystallize and plagioclase of albite composition begin to exsolve out from K-feldspar. The exsolved plagioclase occurs as thin lamellae in K-feldspar and also as thin rims over plagioclase grains in the ocelli.

as a separate immiscible phase. The felsic melt along with immiscible titanite-liquid occupied the low pressure zones constituted by void vesicles. These vesicles were left behind in the mafic system by escaping volatiles/gases. It is to be noted here that the felsic melt had also brought along with it plagioclase grains that were crystallizing in the matrix into the vesicles.

Once the mixture of felsic melt, titanite-liquid and plagioclase crystals occupied the void vesicles, the plagioclase crystals continued to grow with a different composition involving stage 2. At the same time, plagioclase crystals also began to crystallize similar to the new composition.

In stage 3, a few of the crystallizing plagioclase grains (generally one or two) became nuclei or seeds for crystallization of titanite which are presently preserved as inclusions in titanite. The crystallization of titanite over plagioclase prevented further growth of the plagioclase grains present as inclusions in titanite.

Meanwhile in stage 4, as the temperature of the system declined, K-feldspar and quartz began to crystallize and plagioclase of albite composition began to exsolve out from K-feldspar. The exsolved plagioclase occurs as thin lamellae in K-feldspar and also as thin rims over plagioclase grains in the ocelli. However, plagioclase crystals which are present as inclusions in titanite do not show any albite rims indicating that their growth was hindered by titanite crystallization such that they were cut-off from future activities in the vesicle. In this way titanite ocelli formed in a biotite/amphibole rich matrix.

ACKNOWLEDGEMENTS

Ashima Saikia acknowledges the CSIR grant vide Project no. 24(0317)/12/EMR-II and Delhi University Research Grant. Bibhuti Gogoi acknowledges CSIR JRF/SRF fellowship no. 09/045(1146)/2011-EMR1.

APPENDIX

Supplemental material is available for downloading at the journal site.

REFERENCES

Ahmad M., Dubey J., 2011. Report on prospecting for gold and silver mineralization in Munger Rajgir group of rocks in Nalanda District, Bihar. P (ii), Unpublished report, Geological Survey of India (F.S.: 2008-09, 2009-10, 2011-12).

Ahmad M., Paul A.Q., 2012. Tectono-stratigraphic constraints of the Bathani volcano-sedimentary, volcanic sequences and associated rocks, Chotanagpur granite gneiss complex, Gaya district Bihar. NEWS, Geological Survey of India, Eastern region 33, 13-15.

Albaréde F., 1995. Introduction to Geochemical Modeling. Cambridge University Press, Cambridge.

Anderson J.L. and Smith D.R., 1995. The effects of temperature and fO_2 on the Al-in-hornblende barometer. American Mineralogist 8, 549-559.

Baker D.R., 1990. Chemical interdiffusion of dacite and rhyolite: anhydrous measurements at 1 atm and 10 kbar, application of transition state theory to diffusion in zoned magma chambers. Contributions to Mineralogy and Petrology 104, 407-423.

Balaram V., Saxena V.K., Manikyamba C., Ramesh S.L., 1990. Determination of rare earth elements in Japanese rock standards by inductively coupled plasma mass spectrometry. Atomic Spectroscopy 11, 19-23.

Beard J.S., Ragland P.C., Rushmer T., 2003. Dehydration melting reactions and the formation of hydrous phases by incongruent reaction: An alternative way to view the crystallization of hydrous magmas: Geological Society of America, Abstracts with Programs, 35, 92

Beard J.S., Ragland P.C., Rushmer T., 2004. Hydration Crystallization Reactions between Anhydrous Minerals and Hydrous Melt to Yield Amphibole and Biotite in Igneous Rocks: Description and Implications. The Journal of Geology 112, 617-621.

Beard J.S., Ragland P.C., Crawford, M.L., 2005. Reactive bulk assimilation: A model for crust-mantle mixing in silicic magmas. Geology 33, 681-684.

Blake D.H., 1981. Intrusive felsic-mafic net-veined complexes in North Queensland.Australian Bureau of Mineral Resources Geology and Geophysics Bulletin 6, 95-99.

Chappell B.W., White A.J.R., Wyborn D., 1987. The importance of residual source material restite in granite petrogenesis. Journal of Petrology 28, 1111-1138.

Chatterjee N., Ghosh N.C., 2011. Extensive Early Neoproterozoic high-grade metamorphism in North Chotanagpur Gneissic Complex of the Central Indian Tectonic Zone. Gondwana Research 20, 362-379.

Christiansen E.H., Venchiarutti D.A., 1990. Magmatic inclusions in rhyolites of the Spor Mountain Formation, Western Utah: limitations on compositional inferences from inclusions in granitic rocks. Journal of Geophysical Research 95, 17717-17728.

Costa-de-Moura J., Nascimento R.C.C., Wiedemann C.M., Platzer S., Van Westrenen W., Vriend S.P., 1997. The Pedra Azul granite, State of Espírito Santo, SE Brazil, with sphene-centred ocelli: evidence of autometasomatism in a late stage of crystallization. In: Second International Symposium on Granites and Associated Mineralizations. (eds): P. Ferreira-Valderez and A. Sial, 135-136.

Cuesta A., 1991. Petrología granítica del plutón de Caldas de Reis (Pontevedra, España): estructura, mineralogía, geoquímica y petrogénesis (Ser. Nova Terra 5). A Coruña, O Castro.

Dahlquist J.A., 2002. Mafic microgranular enclaves: early segregation from metaluminous magma (Sierra de Chepes), Pampean Ranges, NW Argentina. Journal of South American Earth Sciences 15, 643-655.

Deer W.A., Howie R.A., Zussman J., 1980. An Introduction to the Rock Forming Minerals. 1st Edition (20th Impression), Longman, London, 528 pp.

DePaolo D.J., 1981. Trace element and isotopic effects of combined wall rock assimilation and fractional crystallization. Earthand Planetary Science Letters 53, 189-202.

Didier J. and Barbarin B., 1991. Enclaves and granite petrology. Developments in petrology, 13. Elsevier, Amsterdam.

Droop G.T.R., 1987. A general equation for estimating Fe^{3+} concentrations in ferromagnesian silicates and oxides from microprobe analyses using stoichiometric criteria. Mineralogical Magazine 54, 31-435.

Elburg M.A., 1996. Evidence of isotopic equilibration between microgranitoid enclaves and host granodiorite, Warburton Granodiorite, Lachlan Fold Belt, Australia. Lithos 38, 1-22.

Elburg M.A., Nicholls I.A., Sie S.H., 1995. Mineralogical evidence for the origin of mafic microgranular enclaves in S type granites and volcanics. Nuclear Instruments and Methods in Physics Research B 104, 464-469.

Farner M.J., Lee C.T.A., Putrika K.D., 2014. Mafic-felsic magma mixing limited by reactive processes: A case study of biotite-rich rinds on mafic enclaves. Earth and Planetary Science Letters, 393, 49-59.

Fleet M.E. and Barnett R.L., 1978. $^{IV}Al/^{VI}Al$ partitioning in calciferous amphiboles from the Frood Mine, Sudbury, Ontario. Canadian Mineralogist 16, 527-532.

Foster D.A. and Hyndman D.W., 1990. Magma mixing and mingling between synplutonic mafic dikes and granite in the Idaho-Bitterroot Batholith. In: The nature of cordilleran magmatism. (eds): J.L. Anderson , Geological Society of America Memoir 174, 347-358.

Fourcade S. and Allégre C.J., 1981. Trace elements behaviour in granite genesis; a case study: the calc-alkaline plutonic association from the Quérigut complex (Pyrénées, France). Contributions to Mineralogy and Petrology 76, 177-195.

Frost T.P. and Mahood G.A., 1987. Field, chemical, and physical constraints on mafic-felsic magma interaction in the Lamarck Granodiorite, Sierra Nevada, California. Bulletin of Geological Societyof America 99, 272-291.

Gelman M.L., 1962. Effect of micro-heterogeneity of magmatic melt on the texture of titanium-enriched orbicular diorite. Ann Arbor Geochem 2, 167-175.

Hibbard M.J., 1991. Textural anatomy of twelve magma-mixed granitoid systems. In: Enclaves and Granite Petrology 13. (eds): J. Didier and B. Barbarin, Developments in Petrology, Elsevier, Amsterdam, 431-444.

Hibbard M.J., 1995. Petrography to Petrogenesis. Prentice Hall, New Jersey, pp. 587.

Holden P., Halliday A.N., Stephens W.E., Henney P.J., 1991. Chemical and isotopic evidence for major mass-transfer between mafic enclaves and felsic magma. Chemical Geology 92, 135-152.

Holland T. and Blundy J., 1994. Non-ideal interactions in calcic amphiboles and their bearing on amphibole-plagioclase thermometry. Contributions to Mineralogy and Petrology 116, 433-447.

Ilbeyli N. and Pearce J.A., 2005. Petrogenesis of igneous enclaves in plutonic rocks of the Central Anatolian Massif, Turkey. International Geology Review 47, 1011-1034.

Janoušek V., Braithwaite C.J.R., Bowes D.R., Gerdes A., 2004. Magma mixing in the genesis of Hercynian calc-alkaline granitoids: an integrated petrographic and geochemical study of the Sazava intrusion, Central Bohemian Pluton, Czech Republic. Lithos 78, 67-99.

Johnston A.D. and Wyllie P.J., 1988. Interaction of granitic and basic magmas: experimental observations on contamination processes at 10 kbar with H_2O. Contributions to Mineralogy and Petrology 98, 352-362.

Leake B.E., 1971. On aluminous and edenitic hornblendes. Mineralogical Magazine 38, 389-405.

Leake B.E., Woolley A.R., Arps C.E.S., Birch W.D., Gilbert M.C., Grice J.D., Howthorne F.C., Kato A., Kisch H.J., Krivovichev V.G., Linthout K., Laird J., Mandarino J.A., 1997. Nomenclature of amphiboles. Report of the subcommittee on amphiboles of the International Mineralogical Association: Commission on new mineral names.Mineralogical Magazine 61, 295-321.

McLeod G.W., Dempster T.J., Faithfull J.W., 2011. Deciphering Magma-Mixing Processes Using Zoned Titanite from the Ross of Mull Granite, Scotland. Journal of Petrology 52, 55-82.

Middlemost E.A.K., 1994. Naming materials in the magma/igneous system. Earth Science Reviews 37, 215-224.

Miller C.F., McDowell S.M., Mapes R.W., 2003. Hot and cold granites? Implications of zircon saturation temperatures and preservation of inheritance. Geology 31, 529-532.

Morimoto N., Fabries J., Ferguson A.K., Ginzburg I.V., Ross M., Seifert F.A., Zussman J., Aoki K., Gottardi G., 1988. Nomenclature of pyroxenes. Mineralogy and Petrology 39, 55-76.

Neves S.P. and Vauchez A., 1995. Successive mixing and mingling of magmas in a plutonic complex of Northeast Brazil. Lithos 34, 275-299.

Noyes H.J., Frey F.A., Wones D.R., 1983. A tale of two plutons: geochemical evidence bearing on the origin and differentiation of the Red Lake and Eagle Peak plutons, Central Sierra Nevada, California. Journal of Geology 91, 487-509.

Pietranik A. and Koepke J., 2009. Interactions between dioritic and granodioritic magmas in mingling zones: plagioclase record of mixing, mingling and sub solidus interactions in the Gęsiniec Intrusion, NE Bohemian Massif, SW Poland. Contributions to Mineralogy and Petrology 158, 17-36.

Pin C., Binon N., Belin J.M., Barbarin B., Clemens J.D., 1990. Origin of microgranular enclaves in granitoids-equivocal Sr-Nd evidence from Hercynian rocks in the Massif Central (France). Journal of Geophysical Research 95, 17821-17828.

Pouchou J.L. and Pichoir F., 1987. Basic expressions of PAP computation for quantitative EPMA. Proceedings of ICXOM 11, Ontario, 249-253.

Purohit K.K., Mukherjee P.K., Saini N.K., Khanna P.P., Rathi M.S., 2006. Geochemical Survey of stream sediments from upper parts of Alaknanda, Mandakini, Bhilangana and Bhagirathi Catchments, Garhwal Himalaya. Himalayan Geology 27, 31-39.

Putirka K.D., Mikaelian H., Ryerson F., Shaw H., 2003. New clinopyroxene-liquid thermobarometers for mafic, evolved, and volatile-bearing lava compositions, with applications to lavas from Tibet and the Snake River Plain, Idaho. American Mineralogist 88, 1542-1554.

Putirka K.D., 2008b. Thermometers and barometers for volcanic systems, in: Putirka K.D., and Tepley F. eds., Reviews in Mineralogy Geochemistry. 69, 61-120.

Rieder M., Cavazzini G., D'yakonov J., Kamenetskii F., Gottardi G., Guggenheim S., Koval P., Müller G., Neiva A.M.R., Radoslovich E., Robert J.L., Sassi F.P., Takeda H., Weiss Z., Wones D.R., 1998. Nomenclature of the micas. Canadian Mineralogist 36, 1-8.

Rodríguez J., Vegas N., Esteban J.J., Tubía J.M., 2009. Chemical characterization of igneous sphene and application of the Zr-in-sphene thermometer to tardimagmatic processes. Geogaceta 47, 121-124.

Saikia A., Gogoi B., Ahmad M., Ahmad T., 2014. Geochemical constraints on the evolution of mafic and felsic rocks in the Bathani volcano-sedimentary sequence of Chotanagpur Granite Gneiss Complex. Journal of Earth System Science 123, 959-987.

Saini N.K., Mukherjee P.K., Khanna P.P., Purohit K.K., 2007.

A proposed amphibolite reference rock sample (AM-H) from Himachal Pradesh. Journal of the Geological Society of India 69, 799-802.

Saini N.K., Mukherjee P.K., Rathi M.S., Khanna P.P., 2000. Evaluation of energy-dispersive x-ray fluorescence spectrometry in the rapid analysis of silicate rocks using pressed powder pellets. X-Ray Spectrometry 29, 166-172.

Saini N.K., Mukherjee P.K., Rathi M.S., Khanna P.P., Purohit K.K., 1998. A new geochemical reference sample of granite (DG-H) from Dalhousie, Himachal Himalaya. Journal of the Geological Society of India 52, 603-606.

Tate M.C., Clarke D.B., Heaman L.M., 1997. Progressive hybridisation between Late Devonian mafic-intermediate and felsic magmas in the Meguma Zone of Nova Scotia, Canada. Contributions to Mineralogy and Petrology 126, 401-415.

Tepper J.H. and Kuehner S.M., 2004. Geochemistry of mafic enclaves and host granitoids from the Chilliwack Batholith, Washington: Chemical exchange processes between coexisting mafic and felsic magmas and implications for the interpretation of enclave chemical traits. Journal of Geology 112, 349-367.

Tischendorf, G., Gottesmann B., Förster H.J., Trumbull R.B., 1997. On Li-bearing micas: estimating Li from electron microprobe analyses and improved diagram for graphical representation. Mineralogical Magazine 61, 809-834.

Vegas N., Rodriguez J., Cuevas J., Siebel W., Esteban J.J., Tubía J.M., Basei M., 2011. The Sphene-Centered Ocellar Texture: An Effect of Grain-Supported Flow and Melt Migration in a Hyperdense Magma Mush. Journal of Geology 119, 143-157.

Vernon R.H., 1990. Crystallization and hybridism in microgranitoid enclave magmas: microstructural evidence. Journal of Geophysical Research 95, 17849-17859.

Vernon R.H., 1991. Interpretation of microstructures of microgranitoid enclaves. In: Enclaves and Granite Petrology 13. (eds): J. Didier and B. Barbarin, Developments in Petrology, Elsevier, Amsterdam, 277-291.

Vernon R.H., Etheridge M.A., Wall V.J., 1988. Shape and microstructure of microgranitoid enclaves: indicators of magma mingling and flow. Lithos 22, 1-11.

Waight T.E., Maas R., Nicholls I.A., 2000. Fingerprinting feldspar phenocrysts using crystal isotopic composition stratigraphy: implications for crystal transfer and magma mingling in S-type granites. Contributions to Mineralogy and Petrology 139, 227-239.

Walker F., 1957. Ophitic Texture and Basaltic Crystallization. Journal of Geology 65, 1-14.

Wall V.J., Clemens J.D., Clarke D.B., 1987. Models for granitoid evolution and source compositions. Journal of Geology 95, 731-749.

Watson E.B., Harrison T.M., 1983. Zircon saturation revisited: temperature and compositional effects in a variety of crustal magma types. Earth and Planetary Science Letters 64, 295-304.

Watson E.B. and Jurewicz S.R., 1984. Behavior of alkalies during diffusive interaction of granitic xenoliths with basaltic magma. Journal of Geology 92, 121-131.

White A.J.R. and Chappell B.W., 1977. Ultrametamorphism and granite genesis. Tectonophysics 43, 7-22.

Windley B.F., 1965. The composite net-veined diorite intrusives of the Julianehab district, South Greenland. GEUS Bulletin 58, 1-60.

Xiong F.H., Ma C.Q., Zhang J.Y., Liu B., 2012. The origin of mafic microgranular enclaves and their host granodiorites from East Kunlun, Northern Qinghai-Tibet Plateau: implications for magma mixing during subduction of Paleo-Tethyan lithosphere. Mineralogy and Petrology 104, 211-224.